NSG-198

PLASMA RESEARCH

CASE INSTITUTE OF TECHNOLOGY

UNIVERSITY CIRCLE • CLEVELAND 6, OHIO

A MEASUREMENT OF ENERGETIC TEST ELECTRON INTERACTIONS WITH A PLASMA*

by

Michael R. Smith
W. Bruce Johnson

Technical Report No. A-38

June, 1965

Supported in part by the National Aeronautics and Space Administration

---

*This investigation was submitted in partial fulfillment of the requirements for the degree of Doctor of Philosophy by one of the authors (M. R. S.).

ABSTRACT

An experimental determination is made of the distribution of energy losses suffered by a beam of energetic test electrons traversing a dense, high temperature plasma. The test electron energy is 3,000 electron volts and the plasma density varies from 5×10^{15} to 1×10^{16} cm^{-3} at a temperature of ~ 40,000 ^{o}K . A collisional theory is developed through the ad hoc extension of the maximum impact parameter, $P_{max} = \lambda_D \frac{v}{w_t}$, and agreement is found with the results of various other authors. The experimental average energy loss is larger than the theoretical prediction, indicating a minimum discrepancy of approximately an order of magnitude between theory and experiment. The experimental average energy loss and spread in energy are both found to vary proportional to the plasma electron density. The experimental measurements do not substantiate a proposed energy gain mechanism.

ACKNOWLEDGMENTS

The authors wish to express their appreciation to various colleagues for advice and moral support, to Mr. George Spencer for his help with the spectroscopic system, to Mr. Byron S. Watson for his competent technical assistance, to the Wickenden machine shop for its fine work, to Mr. Doyle Wood of Sylvania for his contribution, and finally to Martha S. Dybas (Mrs.) for typing the manuscript. This work was supported in part by the National Aeronautics and Space Administration.

TABLE OF CONTENTS

TABLE OF CONTENTS

LIST OF ILLUSTRATIONS

LIST OF ILLUSTRATION

CHAPTER I

INTRODUCTION

The problem of the interaction of a test particle with a plasma is a very old problem which has been treated extensively from many standpoints in the literature[1-16]. Interest in this problem has been stimulated primarily by the advent of the controlled thermonuclear program, especially the interaction of test electrons with a plasma through the interest in calculating the phenomenon of "run away" electrons[17,18]. A more basic interest stems from the relationship of this problem to the kinetic theory of ionized gases. Many authors have derived expressions for the energy loss[7-16] of an energetic test electron in a plasma. Kahn[19] has proposed an energy gain mechanism which would apply to the present experimental conditions. Such a phenomenon could accelerate charged particles to the energy necessary for the Fermi mechanism to become operable so as to explain the existence of extremely high energy cosmic rays. If such a process existed it could be a source of energetic protons (~ 1 Mev) which would explain the synthesis of uncommon elements in certain stellar atmospheres[20].

Much of the theoretical and experimental work which has been done in connection with the charged-particle-plasma interaction has been concerned with the plasma interaction of a dense beam of electrons[21,22] rather than with single test electrons. The results

are considerably different and of larger magnitude due to the coherent interaction of the beam particles among themselves. This paper will not be concerned with beam effects. Further complications arise due to applied magnetic fields[18,23]. An excellent review article which contains an extensive bibliography of the theoretical and experimental work on the interaction of charged particles and beams of charged particles with a plasma is presented in reference [21].

The experiment which is described in this report was performed for the purpose of providing an experimental comparison with the various test-electron theories mentioned above. The experimental conditions are described reasonably well by the theoretical models so that a realistic comparison can be made.

A brief summary is given in Chapter II of the present theoretical results obtained for collisional interactions of energetic test electrons with a plasma. These include the derivation of the average energy loss rate, the distribution of energy losses, and the transmission through a plasma. Finally, a brief discussion and comparison of the theories by the various authors is presented. In Chapter III the spectroscopic methods which were used in this experiment for the diagnostics of high temperature plasmas are discussed. Chapter IV contains a description of the experimental apparatus. The results of the experiment are described in Chapter V and a comparison is made with the available theories. Chapter VI

contains a summary of the results and suggestions for future work.

CHAPTER II

THEORETICAL CONSIDERATIONS

2.1 Introduction

An expression for the average rate of energy loss of an energetic electron traversing a plasma in thermal equilibrium is derived* on the assumption that the dominant mechanism for energy loss is the Coulomb interaction. It will further be assumed that the dominant Coulomb interactions for energy loss are electron-electron collisions, since an electron-ion or electron-neutral collision will degrade the electron's energy by a negligible amount. The average energy loss rate is derived in general for an arbitrary distribution of plasma electrons, $f(\underline{w})$. In order to obtain a numerical result $f(\underline{w})$ must be specified. An initial calculation is performed for a stationary plasma with a Maxwellian distribution of electron velocities. This calculation is then extended to the case of a translating plasma with a Maxwellian distribution of electron velocities (this is a model applicable to the plasma behind a moving shock front). The calculation for the average loss rate through a translating plasma indicates that, for laboratory conditions, the effect of the translation is negligible. In a laboratory experiment

*For a complete derivation of the theoretical results presented in this chapter, the reader is referred to Reference [24].

(which will be described in a subsequent chapter) one must usually deal with a beam of electrons rather than a single electron; however, if the beam density is made sufficiently small so that there exists only one beam electron within the interaction volume during the time of the interaction, the beam can be considered as being composed of singly-interacting electrons. An equivalent statement results from specifying that there are many Debye lengths between beam electrons.

Using a binary collision model, a Boltzman equation for the distribution of beam electron energies is derived and solved. The solution describes the distribution of energy losses of an initially monoenergetic electron beam after traversing a finite slab of plasma. The plasma is assumed to have a vacuum boundary. Under the same conditions described above, an expression is derived for the transmission of an energetic electron beam through a finite plasma slab using multiple scattering theory.

2.2 Average Energy Loss for an Energetic Test Electron in a Plasma

The energy loss of an energetic electron of velocity $\underline{v}$ after colliding with a plasma electron of velocity $\underline{w}$ is given by

$$\Delta E(\underline{v}, \underline{w}, \theta_\ell) = \frac{1}{2} m|\underline{v}-\underline{w}|^2 \sin^2 \theta_\ell \qquad (2\text{-}1)$$

where m is the electronic mass and θ_ℓ is the laboratory scattering angle.

The average energy loss per collision is obtained by averaging the typical loss $\Delta E(\underline{v}, \underline{w}, \theta_\ell)$ over the scattering angles θ_ℓ .

$$\Delta E(\underline{v}, \underline{w}) = \frac{1}{\sigma_t} \int_\theta \Delta E(\underline{v}, \underline{w}, \theta_\ell) \, \sigma(\theta_\ell) \, d\Omega_\ell \qquad (2\text{-}2)$$

The weighting function is the Mott-scattering cross section

$$\sigma(\theta_\ell) d\Omega_\ell = \frac{1}{4}\left[\frac{e^2}{\frac{1}{2} m V^2}\right]^2 \left[\frac{1}{\sin^4 \theta_\ell} + \frac{1}{\cos^4 \theta_\ell} - \frac{\cos[(4\pi e^2/hV) \ln \tan \theta_\ell]}{\sin^2 \theta_\ell \cos^2 \theta_\ell}\right] 4 \cos \theta_\ell \, d\Omega_\ell \qquad (2\text{-}3)$$

where $V = |\underline{v} - \underline{w}|$

$d\Omega_\ell = 2\pi \sin \theta_\ell \, d\theta_\ell$.

The total cross section, σ_t is given by

$$\sigma_t = \int \sigma(\theta_\ell) \, d\Omega_\ell$$

and the integration limits are from $\theta_{\ell_{min}}$ to $\theta_{\ell_{max}}$.

The result for $\Delta E(\underline{v}, \underline{w})$ is

$$\Delta E(\underline{v}, \underline{w}) = -\frac{2\pi}{\sigma_t}\left[\frac{1}{2} mV^2 \left(\frac{e^2}{\frac{1}{2} mV^2}\right)^2\right]\left[\ln \frac{\Lambda}{2} - \frac{1}{2}\left(\frac{\Lambda}{2}\right)^{-2} + \ln(\sin \theta_{\ell_{max}}) + \ln(\cos^2 \theta_{\ell_{max}}) + \frac{1}{2} \tan^2 \theta_{\ell_{max}}\right]$$

and $$\Lambda = \frac{2}{\theta_{\ell_{min}}} \quad . \tag{2-4}$$

The deBroglie wave length of the relative motion V is taken as the minimum impact parameter.

$$b_{min} = \lambda = \frac{h}{m|\underline{v}-\underline{w}|} \quad . \tag{2-5}$$

The maximum angle of deflection, $\theta_{\ell_{max}}$, will then be given by the scattering angle corresponding to b_{min}.

$$b_{min} = \frac{e^2}{\frac{1}{2} m|\underline{v}-\underline{w}|^2} \cot \theta_{\ell_{max}} \tag{2-6}$$

or

$$\theta_{\ell_{max}} = \cot^{-1}\left[\frac{h}{m|\underline{v}-\underline{w}|} \frac{1}{2} \frac{m}{e^2} |\underline{v}-\underline{w}|^2 \right] .$$

From the expression for $\theta_{\ell_{max}}$, $\sin \theta_{\ell_{max}}$, $\cos^2 \theta_{\ell_{max}}$, and $\tan^2 \theta_{\ell_{max}}$ can be found. Using these expressions the average energy loss per collision for velocities, $\overline{\underline{v}}$ and $\overline{\underline{w}}$, is given by

$$\Delta E(\underline{v},\underline{w}) = \frac{2\pi}{\sigma_t}\left[\frac{1}{2} mV^2 \left(\frac{e^2}{\frac{1}{2} m V^2} \right)^2 \right]\left[\ell_n \Lambda - \frac{1}{2}\left(\frac{\Lambda}{2} \right)^{-2} \right.$$

$$\left. + \ell_n \frac{2e^2h^2V^2}{(h^2V^2+4e^4)^{3/2}} + 2 \frac{e^4}{h^2V^2} \right] . \tag{2-7}$$

In a small time interval, δt , the number of collisions that the incident electron makes with plasma electrons having velocities in the range $d\underline{w}$ is given by

$$\sigma_t |\underline{v}-\underline{w}| \; \delta t \; f(\underline{w}) \; d\underline{w} \; .$$

The total average energy loss of the incident electron in a time, δt , due to many collisions with plasma electrons in the velocity range, $d\underline{w}$, is

$$\Delta E_{d\underline{w}} = \Delta E(\underline{v}, \underline{w}) \sigma_t |\underline{v}-\underline{w}| \; f(\underline{w}) \; d\underline{w} \; \delta t \; . \qquad (2\text{-}8)$$

Hence the rate of average energy loss becomes

$$\left(\frac{dE}{dt}\right)_{d\underline{w}} = \lim_{\delta t \to 0} \left(\frac{\Delta E}{\delta t}\right)_{d\underline{w}} \; .$$

The total energy loss rate for collisions with plasma electrons of all velocities is obtained by integrating over the plasma electron distribution function, thus

$$\left\langle \frac{dE}{dt} \right\rangle = \int_{\underline{w}} \left(\frac{dE}{dt}\right)_{d\underline{w}} f(\underline{w}) \; d\underline{w} \; .$$

A Maxwellian distribution function is assumed.

$$f(\underline{w}) \; d\underline{w} = \frac{n_e}{\pi^{3/2} \; w_t^3} \exp\left(-\frac{\underline{w} \cdot \underline{w}}{w_t^2}\right) 2\pi w^2 \sin\phi \, d\phi \, dw \qquad (2\text{-}9)$$

where ϕ is the velocity space azimuth angle coordinate for a spherical coordinate system and

$$w_t^2 = \frac{2kT}{m} ,$$

T is the plasma electron temperature, m is the electronic mass, and

$$n_e = \int_{\underline{w}} f(\underline{w})\, d\underline{w} .$$

Carrying out the integration formally the result is obtained in terms of the dimensionless speeds α, β, defined below:

$$\frac{dE}{dt}(\beta) = \frac{-4\pi e^4}{m} \frac{n_e}{w_t} \frac{4}{\sqrt{\pi}} \left[G_1(\beta)+G_2(\beta)+\frac{2e^4}{w_t^2 h^2} G_3(\beta)\right] \qquad (2\text{-}10)$$

where $\alpha = \frac{w}{w_t}$

$$\beta = \frac{v}{w_t} ,$$

and

$$G_1(\beta) = \int_0^\infty \phi_1(\alpha,\beta)\alpha^2 e^{-\alpha^2} d\alpha$$

$$G_2(\beta) = \int_0^\infty \phi_2(\alpha,\beta)\alpha^2 e^{-\alpha^2} d\alpha$$

$$G(\beta) = \int_0^\infty \phi_3(\alpha,\beta)\alpha^2 e^{-\alpha^2} d\alpha ,$$

where the ϕ's are the appropriate averages of the terms in equation 2.7 .

The reader is referred to Reference [24] for details of the evaluation of the G functions. The evaluation of $G_1(\beta)$ requires a value for the minimum laboratory scattering angle in the collision process. This is equivalent to considering the maximum allowable impact parameter. Ordinarily, following Cohen, Spitzer and Routly,[25] the maximum impact parameter would be the Debye radius. Physically the reason for this is that the charged particles in the plasma have adjusted themselves so that the Coulomb potential of the plasma electron has been shielded at distances greater than the Debye length. The result is that the incident electron feels no net potential unless it passes within a Debye length of the plasma electron.

This procedure will give fairly accurate results when the incident electron has a velocity approximately equal to the plasma electron thermal velocity. However, in the present case, where the incident particle velocity exceeds the thermal velocity, the maximum impact parameter must be increased to include correctly the energy lost in polarizing the plasma with the resultant excitation of plasma oscillations. The effect is completely analogous to the Cerenkov effect.

A fast electron can transfer energy to a polarizable medium over a characteristic length which will be taken as the effective maximum impact parameter. The characteristic time of interaction of the fast electron with the plasma is $\frac{b_{max}}{v}$, where b_{max} is the

maximum impact parameter. This time must be of the order of one period of plasma oscillation in order for energy to be transferred to the plasma through polarization. Thus

$$\frac{b}{v} \approx \frac{1}{\omega_p}$$

where ω_p = plasma "frequency". Since

$$\omega_p \approx \frac{w_t}{\lambda_d} \quad ,$$

it follows that

$$b_{max} \approx \frac{v}{w_t} \lambda_d = \beta \lambda_d \quad . \qquad (2\text{-}11)$$

The Debye length must be increased approximately by the factor β to include polarization effects.

The minimum scattering angle can now be written in terms of the maximum impact parameter calculated above. Thus

$$\theta_{\ell,min} = \frac{2}{w_t^3} \sqrt{\frac{32\pi}{m^3}} \left(e^3 n_e^{1/2}\right) \frac{1}{\beta^2 + 2\alpha\beta\mu + \alpha^2} \frac{1}{\beta} \quad . \qquad (2\text{-}12)$$

The scattering angles, $\theta_{\ell,min}$, $\theta_{\ell,max}$, are functions of the relative velocity, $|\underline{v}-\underline{w}|$, and hence depend upon, $\mu = \cos(\underline{v}, \underline{w})$.

The final result for the average energy loss rate becomes

$$\left\langle \frac{dE}{dt} \right\rangle = - \frac{4\pi e^4}{mv} n_e \ln\left[\frac{1}{2} \sqrt{\frac{m^3}{8\pi}} \frac{v^2}{ehn_e^{1/2}} \right] . \qquad (2\text{-}13)$$

If the energy loss in a distance, dx , is much smaller than the incident energy, E , the energy loss rate can be transformed as follows,

$$\frac{1}{v} \frac{dE}{dt} = \frac{dE}{dx}$$

and

$$\left\langle \frac{dE}{dx} \right\rangle = - \frac{2\pi e^4}{E} n_e \ln\left[\frac{1}{\sqrt{8\pi^2}} \frac{E}{\hbar \omega_p} \right] \qquad (2\text{-}14)$$

where $E = \frac{1}{2} mV^2$ and $\omega_p = \left(\frac{4\pi ne^2}{m}\right)^{1/2}$. A plot of $\left\langle \frac{dE}{dx} \right\rangle$ is shown in Figure 2.1 .

The result derived above for the average energy loss rate using a collisional theory through the ad hoc extension of the maximum impact parameter is identical to the results derived by various authors [7-16] . The results of a few different authors are shown in Table 2. The expression for $\left\langle \frac{dE}{dx} \right\rangle$ shown in the table differ only in the choice of minimum impact parameter. For the conditions of the present experiment the deBroglie wave length of the relative motion is larger than the closest distance of approach, b , and hence should be used for the minimum impact parameter.

<dE/dx> for an energetic test electron
traversing a plasma

Fig. 2.1

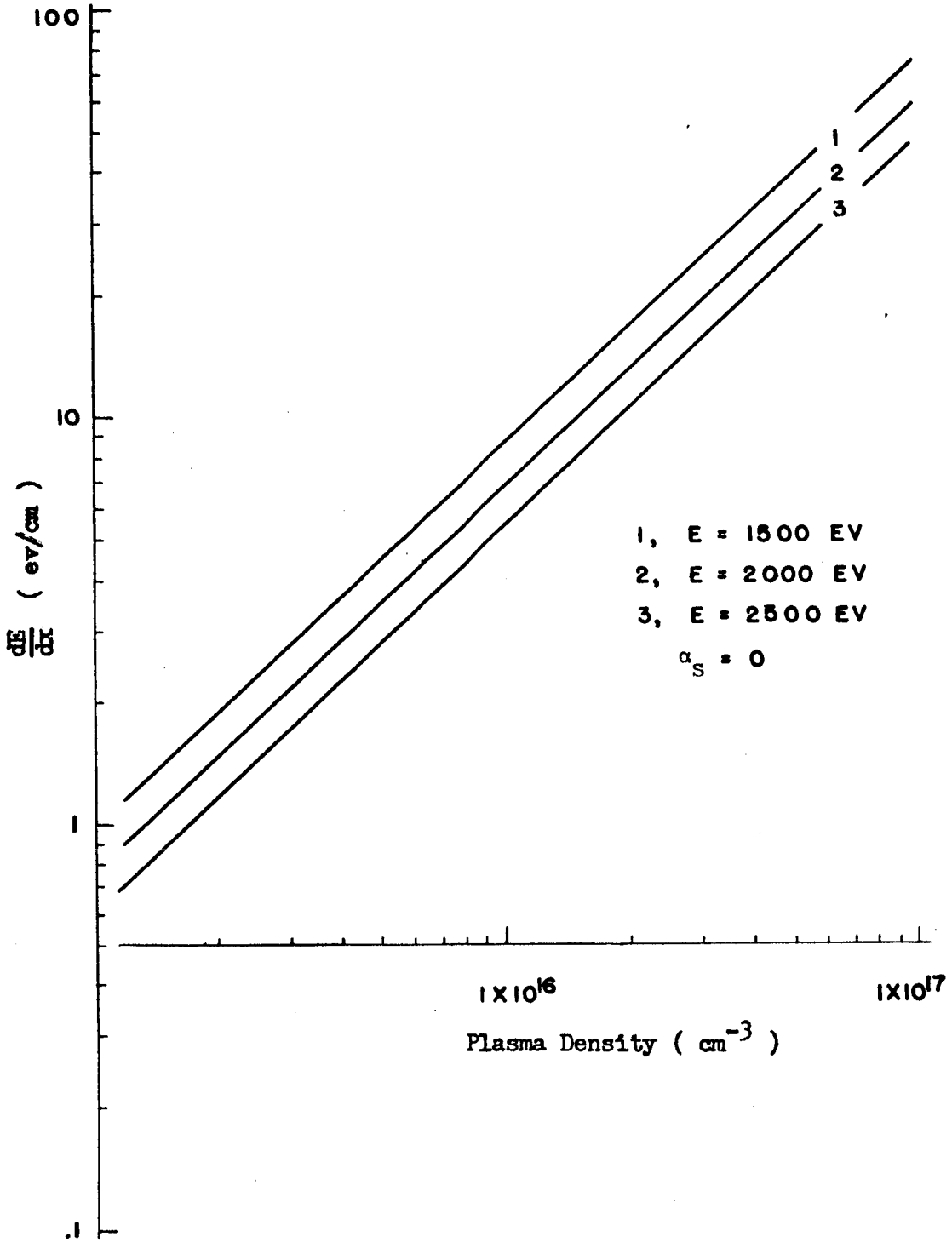
100
10
1
.1
$\frac{dE}{dx}$ (ev/cm)
1, E = 1500 EV
2, E = 2000 EV
3, E = 2500 EV
α_S = 0
1X10^16
1X10^17
Plasma Density (cm^-3)

AUTHOR	dE/dx
Neufeld and Ritchie[8].....	$\frac{2\pi e^4 n}{E} \ln\left(2.246\sqrt{\frac{2}{m}}\ \frac{E^{3/2}}{e^2\omega_p}\right)$
Klimontovich[9]	$\frac{2\pi e^4 n}{E} \ln\left(2\sqrt{\frac{1}{m}}\ \frac{E^{3/2}}{e^2\omega_p}\right)$
Akhiezer[10].....	$\frac{2\pi e^4 n}{E} \ln\left(2.246\sqrt{\frac{2}{m}}\ \frac{E^{3/2}}{e^2\omega_p}\right)$
Pines and Bohm[12].....	$\frac{2\pi e^4 n}{E} \ln\left(2\sqrt{\frac{1}{m}}\ \frac{E^{3/2}}{e^2\omega_p}\right)$
Larkin[13].....	$\frac{2\pi e^4 n}{E} \ln\left(1.36\ \frac{E}{\hbar\omega_p}\right)$
Smith (Present work).....	$\frac{2\pi e^4 n}{E} \ln\left(\frac{1}{\sqrt{8\pi^2}}\ \frac{E}{\hbar\omega_p}\right)$

where n = plasma electron density

E = test particle energy

$\omega_p = \sqrt{\frac{4\pi ne^2}{m}}$ = plasma "frequency"

m = electronic mass

Table 2.

The average energy loss was calculated for a translating, Maxwellian plasma. The result indicates that the energy loss rate in a translating plasma is given by a function, $S(\alpha_S)$, of a dimensionless parameter, α_S , times the energy loss rate in a stationary plasma.

$$\frac{dE}{dx}(\alpha_S) = \frac{dE}{dx}(0)\ S\ (\alpha_S) \qquad (2\text{-}15)$$

The parameter, α_S , is the dimensionless translation speed of the plasma.

$$\alpha_S = \frac{V_S}{w_t}$$

V_S is the translation velocity of the plasma and w_t is the plasma thermal velocity. The function $S(\alpha_S)$ is shown in Figure 2.2 .

2.3 Distribution of Energy Losses

When energetic electrons traverse a layer, x , of plasma, they will lose on the average an energy $\langle \Delta \rangle$. However there will be a statistical fluctuation of energy losses so that on traversal of the slab of plasma an initially monoenergetic electron beam will emerge with a distribution of energy losses which will be denoted by $f(x, \Delta)$, where f is normalized so that

$$\int_{\Delta} f(x, \Delta)\, d\Delta = 1$$

$S(\alpha_3)$ for the effect of the plasma translation on the energy loss

Fig. 2.2

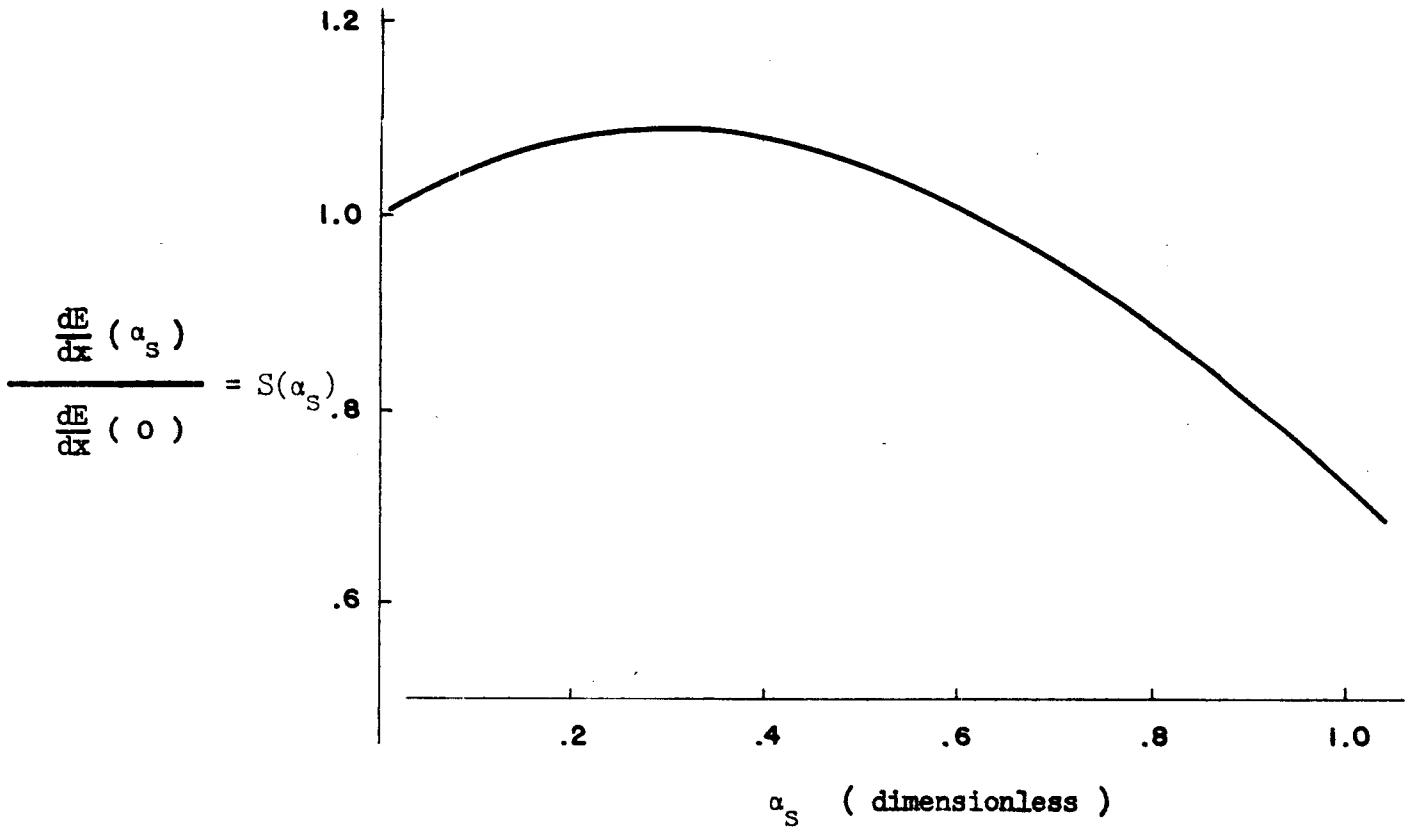
$\frac{\frac{dE}{dx}(\alpha_s)}{\frac{dE}{dx}(0)} = S(\alpha_s)$
1.2
1.0
.8
.6
.2
.4
.6
.8
1.0
α_s (dimensionless)

Let $w(E, \varepsilon)$ be the probability per unit path length that an incident eleetron of energy E will suffer a loss ε. Throughout this calculation it will be assumed that $\varepsilon << E$ so that E will be taken to be constant, E_o.

A kinetic equation for $f(x, \Delta)$ is obtained by equating the change in f along a path length, dx, to the change produced by collisions. The collision integral expresses the difference in the number of particles which acquire, due to collisional losses, an energy, E, and the number of particles which leave the volume in energy space. This is essentially a steady flow Boltzmann equation with no externally applied forces.

$$\frac{\partial f}{\partial x} = \int_o^\infty w(E_o, \varepsilon)[f(x, \Delta-\varepsilon)-f(x, \Delta)]\, d\varepsilon \qquad (2\text{-}16)$$

The probability of losing an energy greater than E_o is zero* so that the upper limit of the integral can be increased to infinity.

Since the kinetic equation does not contain the independent variables x and Δ explicitly, a solution can be obtained by using the Laplaee transform technique. The formal solution is given by[26]

*In this theory energy gain mechanisms are not allowed.

$$f(x,\Delta) = \frac{1}{2\pi i} \int_{-i\infty+\sigma}^{i\infty+\sigma} e^{-s\Delta - x\int_0^\infty w(\varepsilon)[1-e^{-s\varepsilon}]d\varepsilon} ds \qquad (2\text{-}17)$$

where s is the Laplace transform variable. The initial condition for $f(0,\Delta)$ is chosen to be a delta function $f(0,\Delta) = \delta(0)$. The inverse transform is carried out along a line parallel to the imaginary axis of the complex plane and shifted to the right by $\sigma > 0$.

The probability of energy loss, $w(\varepsilon)$, can be derived from the cross section for energy loss [3]. The differential cross section for an energy loss, ε, is given by

$$d\sigma = \frac{\pi e^4}{E} \frac{d\varepsilon}{\varepsilon^2} \qquad (2\text{-}18)$$

where ε is the energy loss of the test electron of energy, E,. It is assumed that the test electron is considerably more energetic than the plasma electron. The probability of losing an energy between ε and $\varepsilon+d\varepsilon$ per collision is

$$\frac{d\sigma}{\sigma_t} = \frac{1}{\sigma_t} \frac{\pi e^4}{E} \frac{d\varepsilon}{\varepsilon^2}$$

where σ_t is the total cross section for energy loss and is given by

$$\sigma_t = \frac{\pi e^4}{E} \int_{\varepsilon_{min}}^{\varepsilon_{max}} \varepsilon^{-2}\, d\varepsilon \ .$$

The number of collisions per unit length traversed by the test electron is $\sigma_t n_e$; so that the probability of losing an energy between ε and $\varepsilon+d\varepsilon$ per unit length of travel is

$$w(\varepsilon)d\varepsilon = \frac{\pi e^4 n_e}{E} \frac{d\varepsilon}{\varepsilon^2} \quad . \tag{2-19}$$

Performing the integrations, the solution for $f(x, \Delta)$ reduces to

$$f(x, \Delta) = \frac{1}{\xi} \phi(\lambda) \tag{2-20}$$

where $$\phi(\lambda) = \frac{1}{2\pi i} \int_{-i\infty+\sigma}^{i\infty+\sigma} e^{v\ell nv+\lambda v} \, dv \tag{2-21}$$

and $$v = \xi s$$

$$\lambda = \frac{\Delta - \xi(\ell n \, \xi/\varepsilon_{min} + 1 - c)}{\xi} \tag{2-22}$$

$$\xi = x \frac{\pi e^4 n_e}{E} \tag{2-23}$$

and $c = 0.577$ is Euler's constant.

The distribution of energy losses, f , is found to be $\frac{1}{\xi}$ times a universal function of a dimensionless parameter λ . The function $\phi(\lambda)$, shown in Figure 2.3 , is given by Landau in his paper[26] . The function has a maximum at $\lambda = -.05$ so that the most probably energy loss is given by (see Figure 2.3a)

Landau's universal function, $\phi(\lambda)$

Fig. 2.3

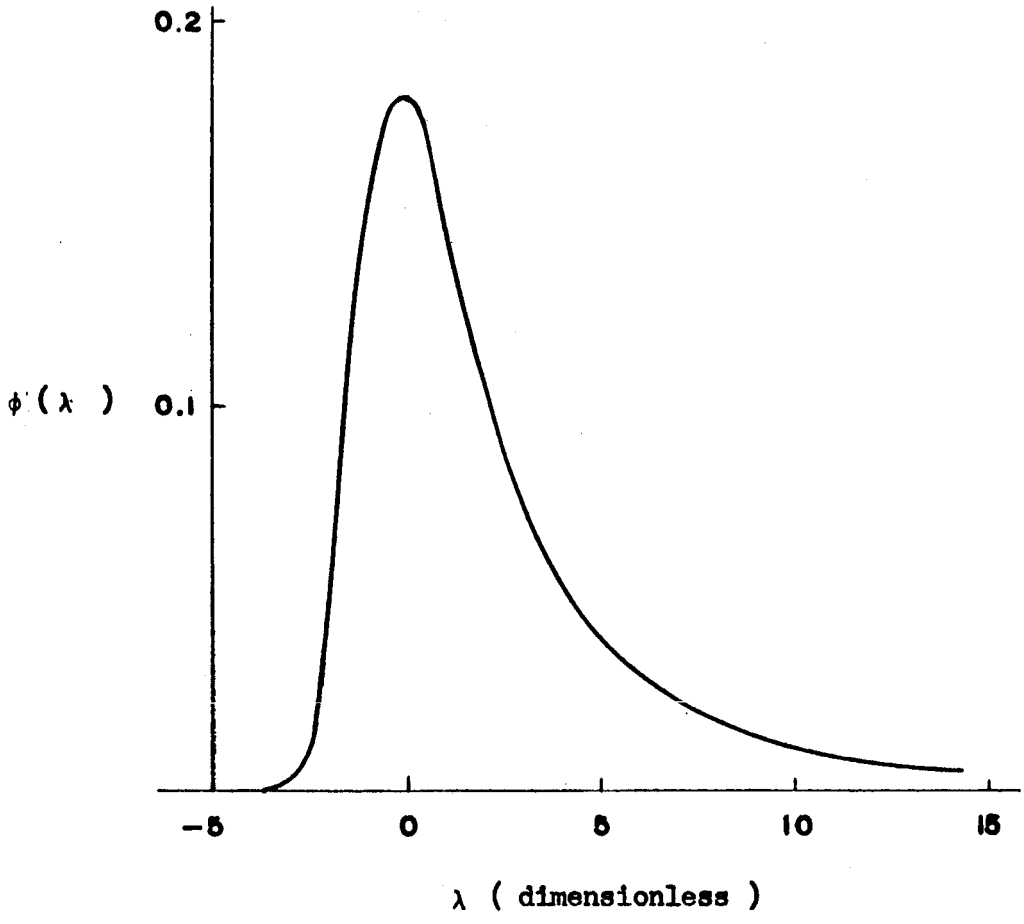
0.2
0.1
$\phi(\lambda)$
-5
0
5
10
15
λ (dimensionless)

Most probable energy loss as a function
of beam energy and plasma density

Fig. 2.3a

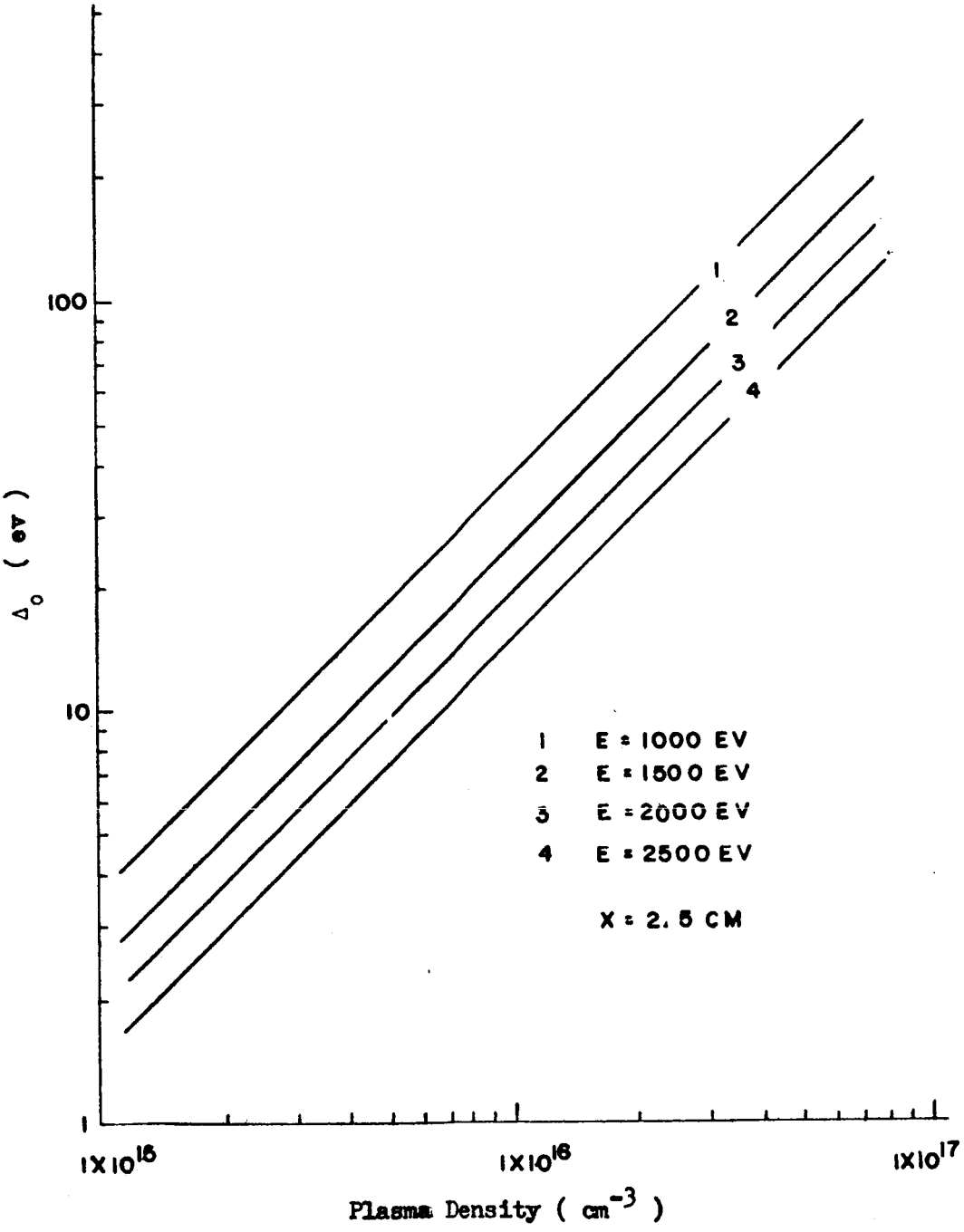
100
10
1
Δ_o (ev)
1
2
3
4
1 E = 1000 EV
2 E = 1500 EV
3 E = 2000 EV
4 E = 2500 EV
X = 2.5 CM
1X10^15
1X10^16
1X10^17
Plasma Density (cm^-3)

$$\Delta_o = \xi\left(\ell n \frac{\xi}{\epsilon_{min}} + 0.37\right) \quad . \qquad (2\text{-}24)$$

A plot of $f(x, \Delta)$ as a function of plasma electron density, electron beam energy, and distance traversed is shown in Figure 2.4, and Figure 2.5 .

The solution which has been obtained describes the interaction of an initially monoenergetic beam of energetic test electrons traversing a plasma. It is important to note that the spreading in energy of the test particles does not depend upon a temperature for the test particles since, in fact, they have been assumed to enter with zero temperature (delta function initial condition). The spreading in energy emerges from the solution of the Boltzmann equation and is due physically to the binary collisions which were assumed as the model. In each binary collision there is a possible variation of energy losses due to collisions at different angles. Most of the collisions occur at very small scattering angles so that the spread in energy losses should be small and, indeed, the solution indicates that this is the case (see Figure 2.5) .

Energy relaxation of an energetic test electron beam in a plasma

Fig. 2.4

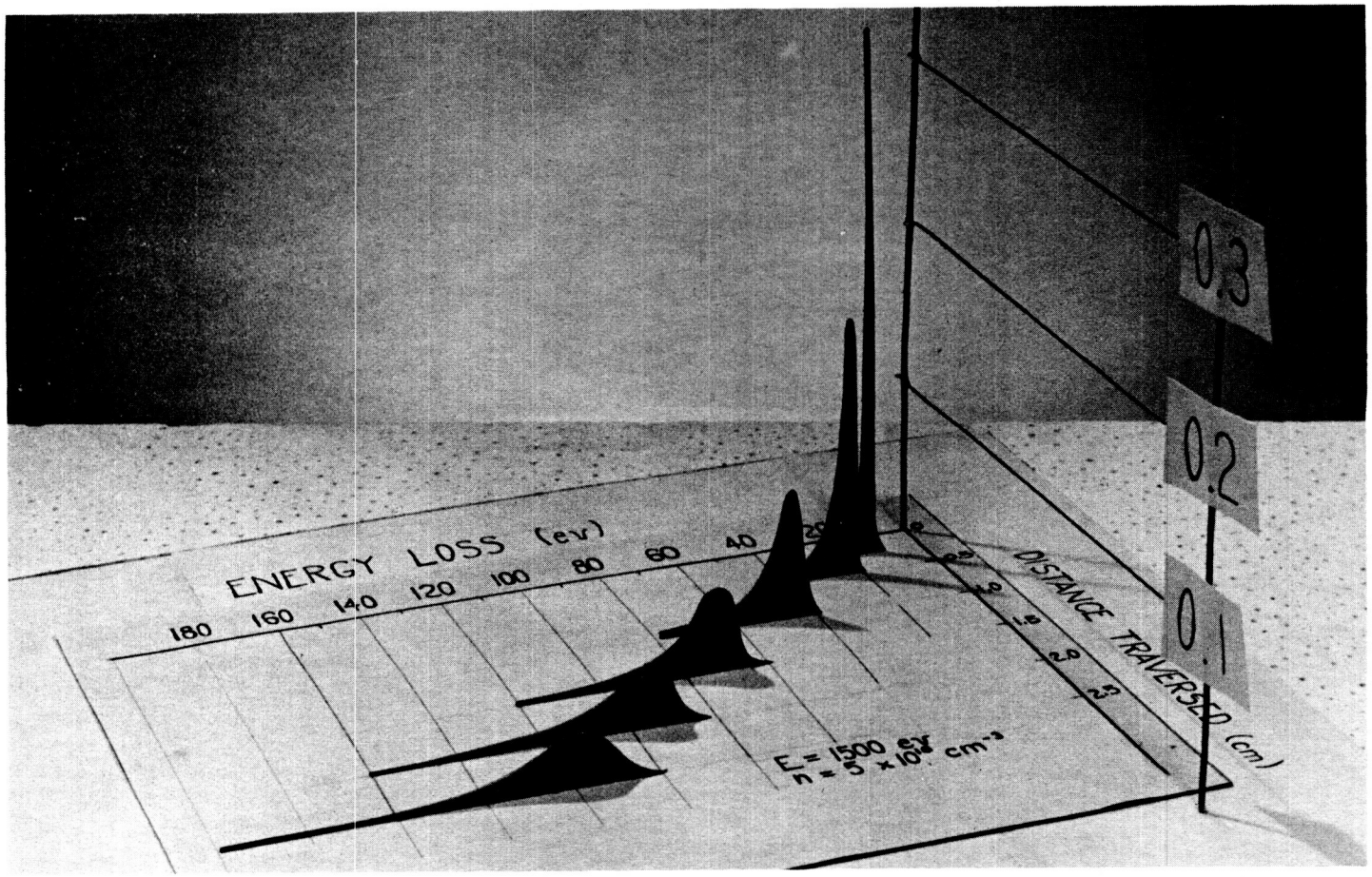
ENERGY LOSS (ev)
180
160
140
120
100
80
60
40
DISTANCE TRAVERSED (cm)
0.3
0.2
0.1
E = 1500 ev
n = 5 x 10^16 cm^-3

Distribution of energy losses as a function of electron density for 1500 ev test electrons

Fig. 2.5

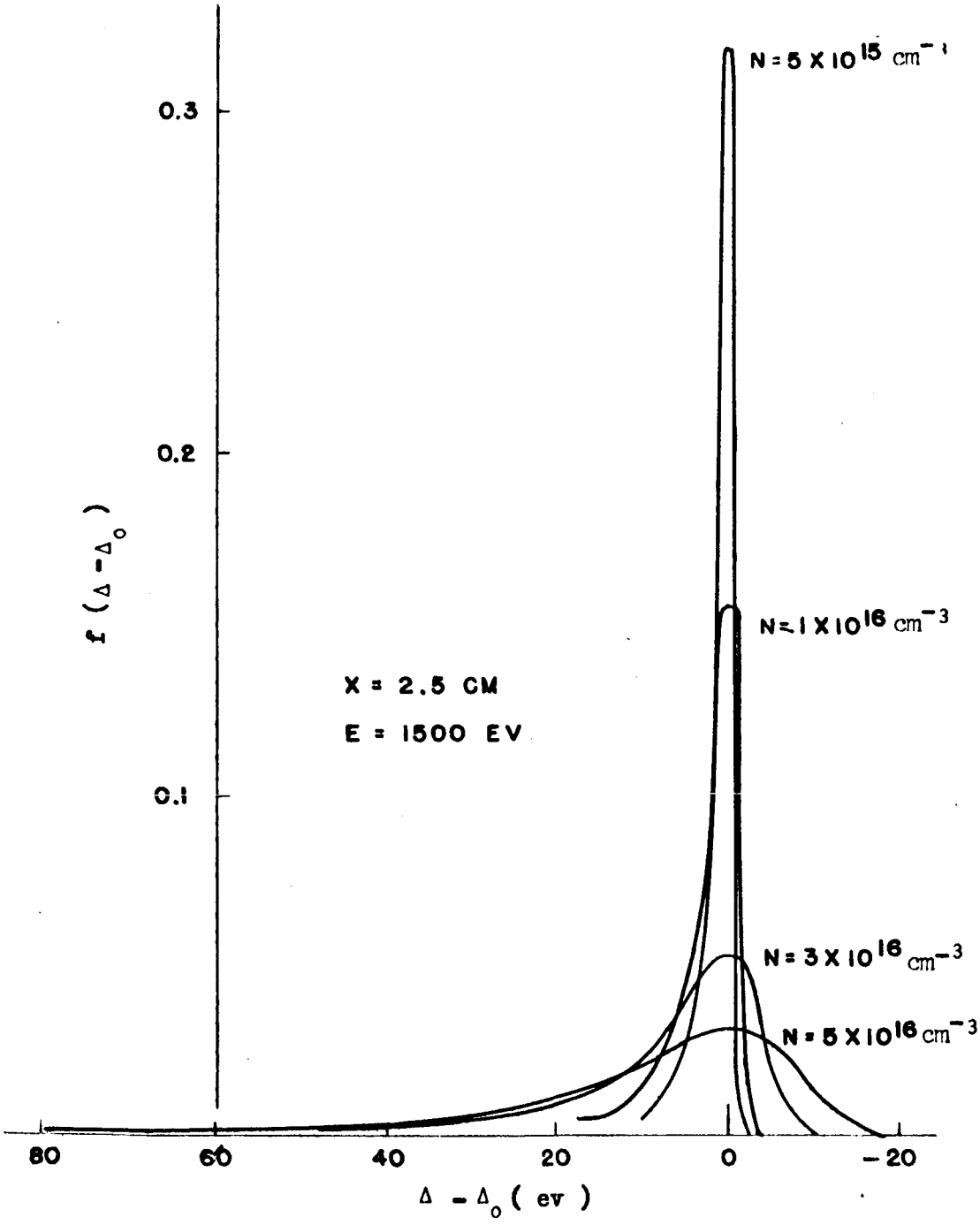
N = 5 X 10^15 cm^-3
N = 1 X 10^16 cm^-3
N = 3 X 10^16 cm^-3
N = 5 X 10^16 cm^-3
X = 2.5 CM
E = 1500 EV
f (Δ - Δ0)
0.3
0.2
0.1
80
60
40
20
0
-20
Δ - Δ0 (ev)

2.4 Transmission of the Electron Beam

When an energetic test electron traverses a slab of dense plasma, the test electron experiences a large number of small angle scatterings resulting in a net angular deviation from its original trajectory. Since the individual scatterings are at small angles, $\theta_i << 1$, the problem can be treated statistically in a reasonably simple manner.[7] For small scattering angles, multiple scattering theory predicts an accumulated deflection angle, θ, distributed about $\theta=0$ according to a Gaussian law. θ is measured from the entrance plane of the beam. Thus

$$p(\theta)\, d\theta = \text{const.} \exp\left(-\frac{\theta^2}{\langle\theta^2\rangle}\right) d\theta$$

where $p(\theta)\, d\theta$ is the probability of realizing a net deflection angle between θ and $\theta + d\theta$, and $\langle\theta^2\rangle$ is the average squared, accumulated deflection angle. This is equivalent to the statement that a beam of independently interacting test particles will have an emergent current distribution (provided the energy change of the particles is small, i.e., $\Delta E << E_o$) given by

$$j(\theta)\, d\theta = \text{const.} \exp\left(-\frac{\theta^2}{\langle\theta^2\rangle}\right) d\theta \qquad (2\text{-}25)$$

where $j d\theta$ is the beam current emerging between an angle of θ and $\theta+d\theta$. Solving for the constant,

$$j(\theta)\, d\theta = \frac{J_o}{\left(\frac{\pi}{2}\langle\theta^2\rangle\right)^{1/2} \operatorname{erf}\left(\frac{\pi}{2}/\langle\theta^2\rangle^{1/2}\right)} \exp\left(-\frac{\theta^2}{\langle\theta^2\rangle}\right) d\theta\,, \qquad (2\text{-}26)$$

where J_o is the incident beam current and

$$\int_0^{\pi/2} e^{-\frac{\theta^2}{\langle\theta^2\rangle}} d\theta = \left(\frac{\pi}{2}\langle\theta^2\rangle\right)^{1/2} \operatorname{erf}\left[\frac{\pi}{2}\left(\frac{1}{\langle\theta^2\rangle}\right)^{1/2}\right] .$$

The transmission of the beam through an exit aperture defined by θ_o (see Figure 2.6) is calculated by taking the ratio of the beam current exiting through θ_o to the total incident beam current, J_o. A diagram of the transmission is shown in Figure 2.6 .

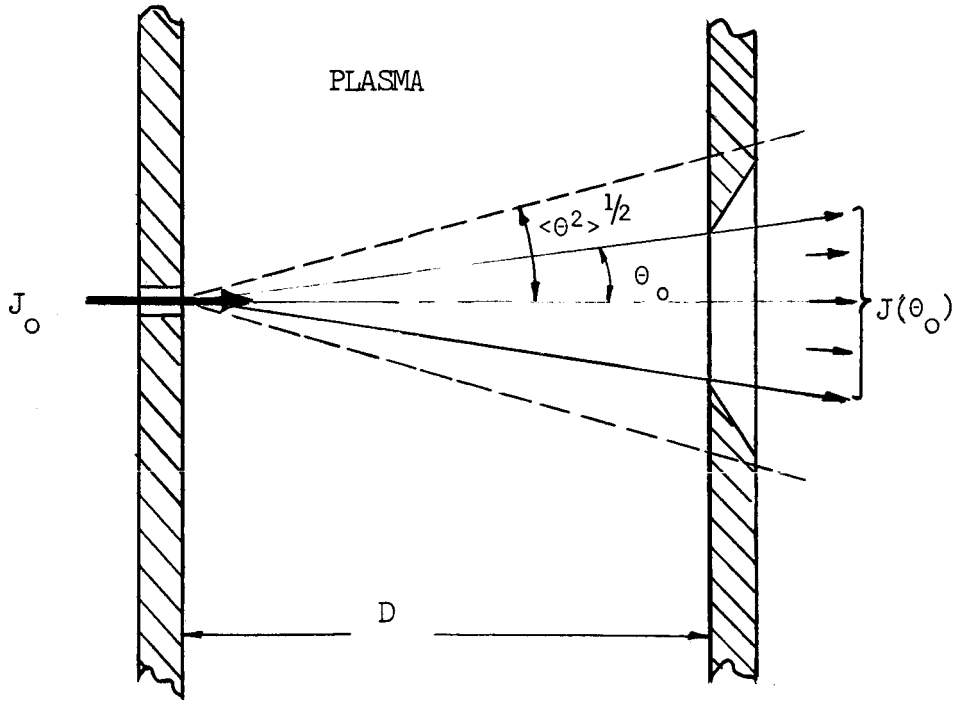

Fig. 2.6 Diagram of Beam Transmission

Then the transmission is given by

$$T = \frac{J(\theta_o)}{J_o} = \frac{\mathrm{erf}(\theta_o/\langle\theta^2\rangle^{1/2})}{\mathrm{erf}(\pi/2/\langle\theta^2\rangle^{1/2})} \qquad (2\text{-}27$$

where the total current J_o is given by

$$J_o = J(\pi/2) \ . \qquad (2\text{-}28)$$

The average squared, accumulated deflection angle, $\langle\theta^2\rangle$ is equal to the average squared deflection angle per collision times the total number of collisions. Thus,

$$\langle\theta^2\rangle = P\langle\theta^2\rangle \ , \qquad (2\text{-}29)$$

where P is the average number of collisions in a single traversal of the plasma slab and $\langle\theta^2\rangle$ is the average squared angle of deflection per collision. For small angle collisions $P = \sigma_t Dn$, where σ_t is the total scattering cross section and is given in terms of the impact parameter by

$$\sigma_t = \int_{x_{min}}^{x_{max}} 2\pi \, x \, dx \ .$$

D is the distance traversed, and n is the plasma eleetron density. Performing the integration,

$$P = 2\pi \, Dn \, \frac{1}{2}(x_{max}^2 - x_{min}^2) \ . \qquad (2\text{-}30)$$

The maximum impact parameter is the dominant term and

$x^2_{max} = (\lambda_D \frac{v}{w_t})^2$, where λ_D is the Debye radius, v is the test electron speed and w_t is the most probable plasma electron speed. Substituting the expression for λ_D and w_t ,

$$P = DE/2e^2 \ , \qquad (2\text{-}31)$$

where $E = \frac{1}{2}mv^2$.

The value for $<\theta^2>$ per collision is calculated by averaging θ^2 over the scattering cross section for θ . The Rutherford scattering cross section is used.

$$<\theta^2> = \frac{1}{\sigma_t}\int_{\theta_{min}}^{\theta_{max}} \theta^2 \, d\sigma(\theta) = \frac{1}{\sigma_t}\frac{2\pi e^4}{E^2}\int_{\theta_{min}}^{\theta_{max}} \frac{\theta^2}{\sin^4\theta} \sin\theta \cos\theta \, d\theta \qquad (2\text{-}32)$$

Making a small angle approximation, $\sin\theta \approx \theta$, the result is

$$<\theta^2> \approx \frac{1}{\sigma_t}\frac{2\pi e^4}{E^2}\int_{\theta_{min}}^{\theta_{max}} \frac{d\theta}{\theta} = \frac{1}{\sigma_t}\frac{2\pi e^4}{E^2} \ln\frac{\theta_{max}}{2}\Lambda \qquad (2\text{-}33)$$

where $\theta_{max} = \frac{2e^2}{hv}$

$\theta_{min} \equiv 2/\Lambda$.

The total cross section* is related to the average number of collisions in one traversal of the slab by

$$\sigma_t = \frac{P}{nD} = \frac{1}{2} \frac{E}{n_e^2} , \qquad (2\text{-}34)$$

and

$$\langle \theta^2 \rangle = \frac{4\pi e^6}{E^3} n\ell n\left(\frac{1}{2\pi \sqrt{2}} \frac{E}{\hbar\omega_p} \right) . \qquad (2\text{-}35)$$

Finally, the average squared, accumulated deflection angle is given by

$$\langle \theta^2 \rangle = P\langle \theta^2 \rangle = \frac{2\pi e^4}{E^2} nD\ell n\left(\frac{1}{2\pi\sqrt{2}} \frac{E}{\hbar\omega_p}\right) . \qquad (2\text{-}36)$$

A calculation of the scattering due to ions proceeds in complete analogy to the electron scattering calculation. The result is that the ions contribute another equal contribution to the scattering of the beam. Since the multiple scattering profile is Gaussian in shape, the effect of the ions is included in the beam transmission result by increasing the average squared, accumulated deflection angle by the factor two.

---

*The total cross section for an inverse-square law interaction potential as derived above has a peculiar dependence on energy and density. In fact, the dependence is the reciprocal of what one would expect, $\sigma_t \sim E/n$. The reason for this peculiar dependence is that the total Coulomb interaction cross section owes its magnitude to the small angle encounters and these are more numerous for a tenuous plasma and a high velocity test particle.

CHAPTER III

DIAGNOSTICS OF HIGH TEMPERATURE PLASMAS

The temperature of a plasma can be determined by making a relative line to continuum intensity measurement. Under the conditions of local thermodynamic equilibrium (LTE), the Saha equation can be used to relate the number density in the upper state of the line to the density of ions and electrons.

$$\frac{I^o}{I_c} = F(T) \tag{3-1}$$

The result is independent of density. The atomic line radiation is given by

$$I^o_{if} = n_o \frac{h\nu_{if}}{4\pi} \frac{g_i}{z_o} A_{if} e^{-\frac{E_i}{kT}} \tag{3-2}$$

where $h\nu_{if}$ is the energy of the transition, g_i is the statistical weight of the initial state, z_o is the total partition function, A_{if} is the transition probability, and n_o is the total atom density. The Saha equation is

$$\frac{n_e n_+}{n_o} = 2 \frac{z_+}{z_o} \left(\frac{2\pi m_e kT}{h^2}\right)^{3/2} \exp\left(\frac{E^i}{kT}\right) \tag{3-3}$$

where E^i is the atomic ionization potential. The continuum formula is

in equation (3-4).

The electron density in a plasma can be obtained independently from the measurement of Stark-broadened line profiles and from absolute continuum intensity measurements. Earlier work by Berg, et.al.[27], using a T-type shock tube and Weise, et. al.[28], using a high current stabilized arc have shown that these two methods yield electron densities which agree to within 5% .

The absolute intensity of the continuum radiation per unit wave length interval, $\Delta\lambda$, from a hydrogen plasma of thickness, ℓ , is given by

$$I_c = 6.36\times10^{-62}\,\frac{c}{\lambda^2}\,\frac{n_e^2}{(kT)^{1/2}}\,\ell\,\exp\left(-\frac{h\nu}{kT}\right)\left[g_{ff}\exp\left(\frac{h\nu_g}{kT}\right)\right.$$

$$\left. + 2\frac{E_{iH}}{kT}\Sigma\,\frac{g_{fb}}{n^3}\exp\left(\frac{E'_n}{kT}\right)\right]\exp\left(-\frac{\Delta I_i^o}{kT}\right) \qquad (3\text{-}4)$$

$$\left[\frac{\text{Watts}}{\text{cm}^2\text{- sr- Ang}}\right]$$

with the quasi-neutrality condition being $n_e = n_i$. T is the electron temperature, $h\nu_g$ is the energy difference between the last observed discrete level and the theoretical series limit, E_{iH} is the ionization energy, g_{ff} and g_{fb} are the Gaunt factors for free-free end free-bound transitions,[29] respectively, and the

summation is taken over all continua with lower states E_n' which contribute at the frequency ν . The term $\exp(-\Delta I_i^o/kT)$ represents a correction for the reduction in the ionization energy at high electron densities,[30] which is of the order of 5% . For non-hydrogenic behavior, such as the continuum from Helium, corrections must be made to hydrogenic relations[31] . These corrections are relatively small, being in the order of 20% for the absolute value of the continuum. Under quasi-neutrality conditions the continuum intensity is proportional to the square of the electron density and therefore the eleetron density can be calculated with approximately twice the accuracy as the combined experimental and theoretical accuracy of absolute continuum intensities.

Measured Stark profiles permit the determination of electron densities in plasmas of almost any chemical composition. Comparison of theoretical Stark profiles with experiments indicate that the calculated half-widths are reliable to within 10 per cent for HeI lines.[31] A standard procedure for determining electron densities from Stark broadening is based on the comparison of measured and calculated full line widths at half maximum intensity. Calculated parameters, by which the line widths can be computed, are tabulated in Griem.[31]

CHAPTER IV

EXPERIMENTAL APPARATUS

4.1 Introduction

The apparatus used for the experimental study of energetic test electron interactions with a plasma consists of the following components: an electromagnetic shock tube to produce a dense, high temperature plasma; an electron gun to generate a low density beam of energetic test electrons; a differential pumping system to allow access of the electron beam into the plasma while maintaining the necessary operating pressures; an energy analyzer to measure the distribution of energies of the emergent electron beam; a spectroscopic analysis system to determine the plasma temperature and density; and finally, a data recording system, to monitor the spectroscopic and energy analysis data. A photograph of the experimental apparatus is shown in Figure 4.1 .

4.2 Plasma Source

A laboratory plasma is obtained by means of an electromagnetic shock tube, more commonly called a "T" tube [32] . The simplicity, reliability, and reproducibility of the "T" tube make it an extremely convenient source of dense, high temperature, laboratory plasma. The tube used in this experiment is constructed from 1 in. ID, precision bore, Pyrex glass tubing. The driver section of the "T" tube consists of a heavy wall, Pyrex glass tee with hemispherical, stainless steel electrodes epoxyed into the ends of the tee. The downstream end of

Photograph of the experimental apparatus

Fig. 4.1

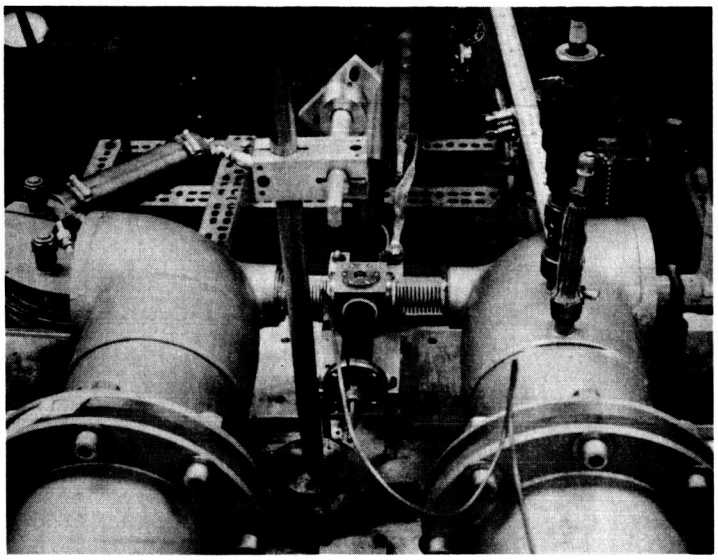

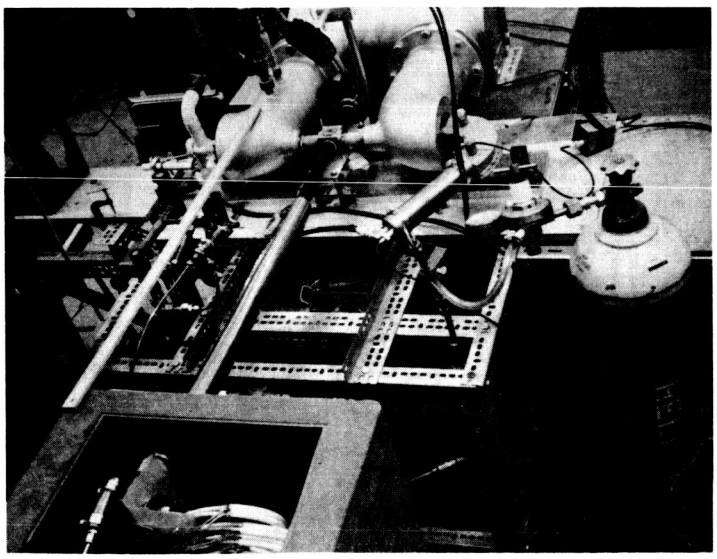

the shock tube is epoxyed into the "scattering block", and the stainless steel scattering block contains apertures for the electron beam and for the spectroscopic measurements. It is located 100 cm downstream from the driver section. A brass, shock reflector is placed 5 mm downstream from the electron beam apertures. An access port located in the side of the tee allows the working gas to enter the tube. Helium gas is used at an ambient tube pressure of .35 torr. A 14.7 mfd low inductance capacitor is connected to the bottom electrode through two ignitron switches connected in parallel. The capacitor is normally charged to 10-15 KV. In order to avoid a discharge current from the electrodes to the grounded scattering block, the electrodes are isolated through 50K resistors to ground. An overall drawing of the shock tube and differential pumping system is shown in Figure 4.2 . The circuit diagram for the ignitron trigger circuit is shown in Figure 4.3 .

4.3 Differential Pumping System

A differential pumping system is required to maintain the shock tube at the operating pressure of .35 torr and the electron gun at 10^{-5} torr while providing an entry for the electron beam into and out of the plasma. At pressures higher than 1×10^{-4} torr, the oxide coated cathode of the electron gun is destroyed by positive ion bombardment. A photograph of the effects of increasing degrees of positive ion bombardment of the cathode is shown in Figure 4.4 . The electron gun and the energy analyzer are connected to the shock tube through two drift tubes, located behind the electron beam apertures

Drawing of the shock tube and the differential pumping system

Fig. 4.2

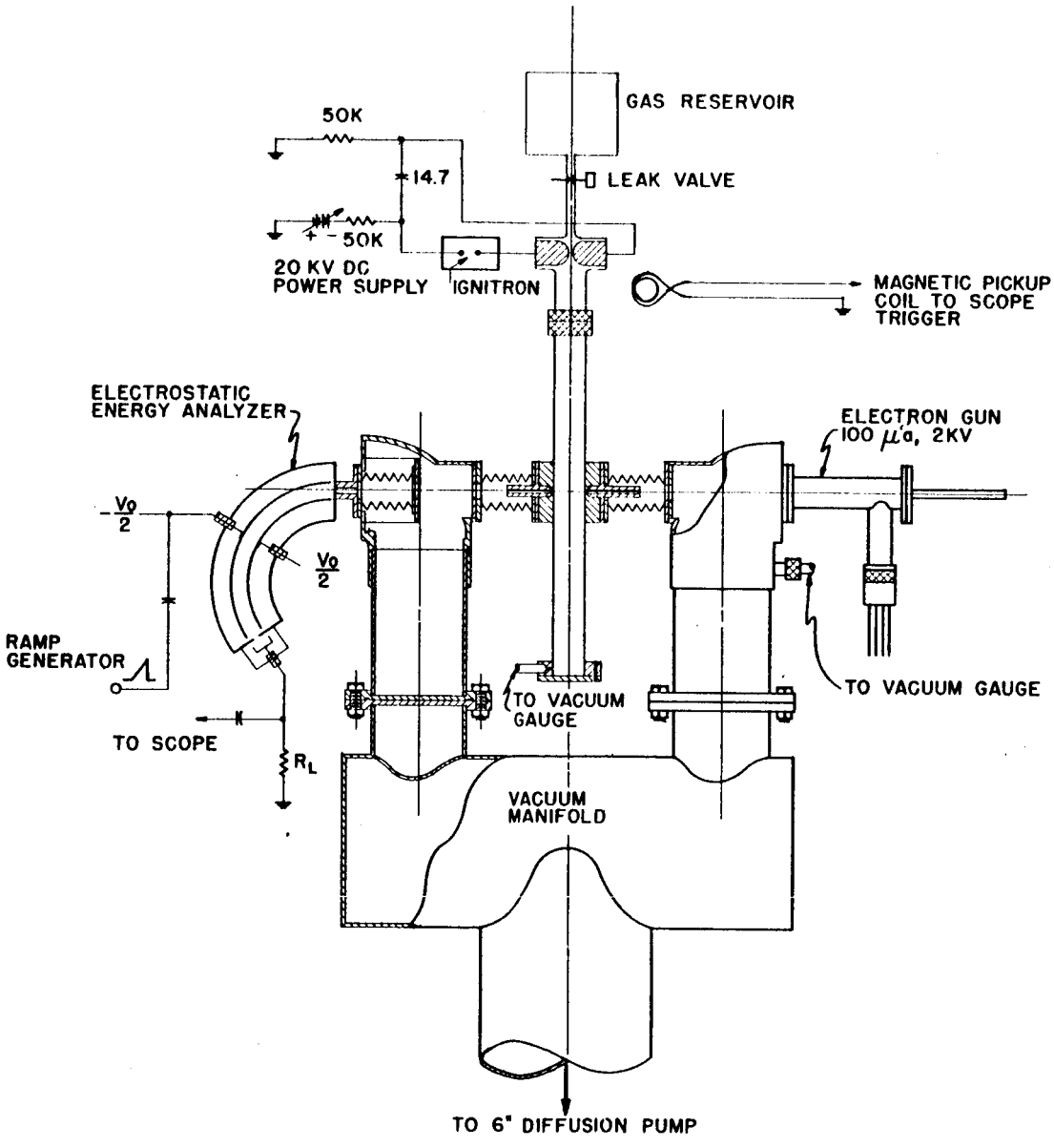
GAS RESERVOIR
50K
14.7
LEAK VALVE
+ - 50K
20 KV DC
POWER SUPPLY
IGNITRON
MAGNETIC PICKUP
COIL TO SCOPE
TRIGGER
ELECTROSTATIC
ENERGY ANALYZER
ELECTRON GUN
100 μa, 2KV
$-\frac{V_0}{2}$
$\frac{V_0}{2}$
RAMP
GENERATOR
TO VACUUM GAUGE
TO VACUUM
GAUGE
TO SCOPE
R_L
VACUUM
MANIFOLD
TO 6" DIFFUSION PUMP

Ignitron trigger circuit

Fig. 4.3

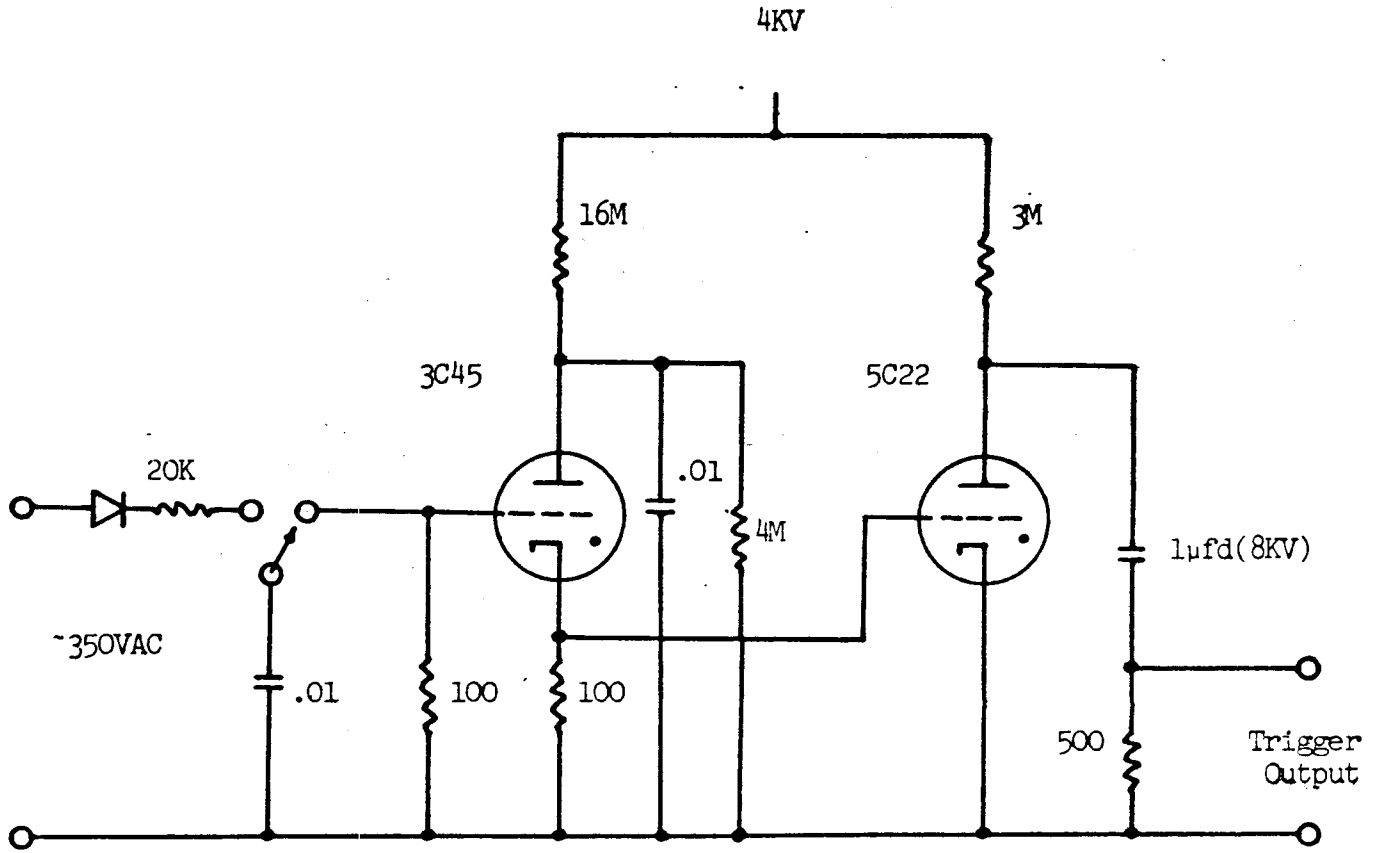
4KV
16M
3M
3C45
5C22
20K
.01
4M
1μfd(8KV)
~350VAC
.01
100
100
500
Trigger
Output

Photograph showing various stages of positive ion bombardment of the oxide coated cathode

Fig. 4.4

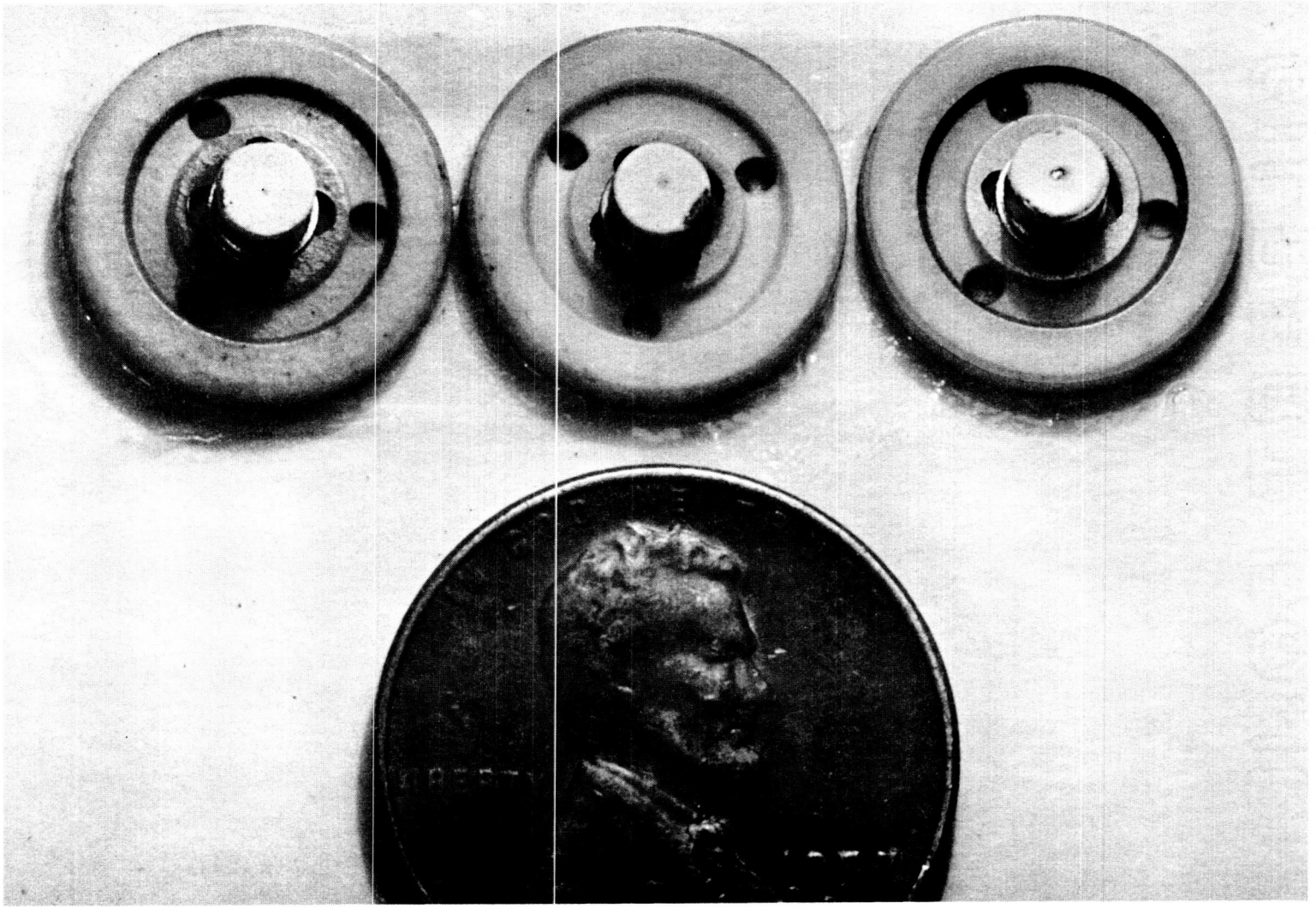

in the scattering block (see Figure 4.5). The drift tubes have a 1/16 in diameter hole and are 2 in long. A 6 in diffusion pump is connected to the drift tubes through a vacuum manifold system consisting of an 8 in diameter riser connecting the pump to the manifold, followed by two 6 in headers which connect to the drift tubes. In the operation of the system, helium is admitted to the shock tube from a low pressure reservoir through an adjustable leak valve. A steady flow is established with the gas expanding, from .35 torr in the shock tube, through the drift tubes to a pressure of 10^{-5} torr. The diffusion pump maintains the low pressure by pumping the gas out at a rate of 2000 l/sec at 10^{-5} torr. The diffusion pump is followed by a 10 cu. ft./min. mechanical pump. The static gas pressure in the shock tube is measured with a McLeod guage.

4.4 Electron Gun

A low current source of 1-3 kev electrons is provided by a commercial cathode ray electron gun. A photograph of the gun is shown in Figure 4.6 . The gun is of the electrostatic, three ring focusing type with an oxide coated cathode. Typical beam currents range from 100 to 300 μa with a heater current of 600 to 650 ma at 6.3 volts. The electron gun is operated in the following manner. The intensity control grid is always maintained at cathode potential. The accelerator grid is operated at +350 volts with respect to the cathode and the focus voltage varies $\pm$50 volts about the cathode potential depending upon the value of the cathode potential (the focus voltage is approximately 0 volts for -3KV cathode potential).

Detail drawing of the drift tubes

Fig. 4.5

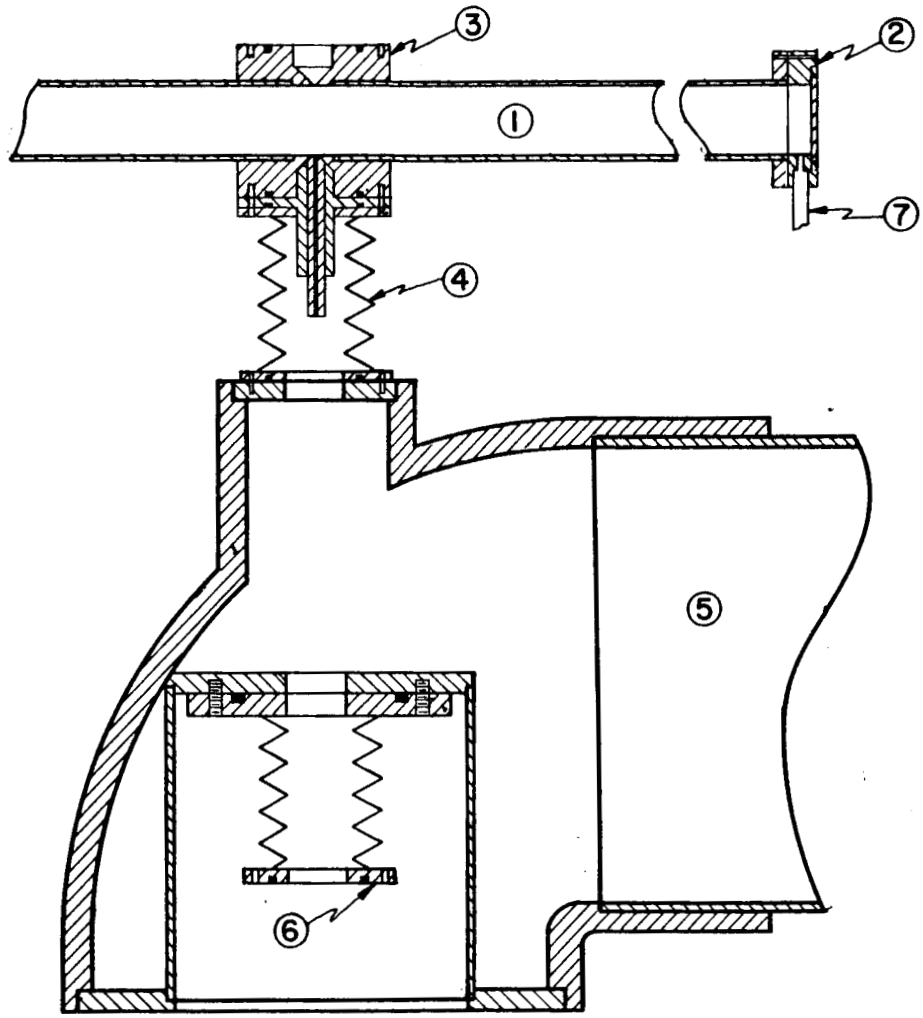

① SHOCK TUBE
② END PLATE
③ SCATTERING BLOCK
④ DRIFT TUBE ASSEMBLY
⑤ VACUUM PUMP LINE
⑥ CONNECTION TO ELECTRON GUN OR ENERGY ANALYZER
⑦ PRESSURE GAUGE CONNECTION

Photograph of the electron gun showing the location of: (a) cathode and heater, (b) beam intensity control grid, (c) accelerator grid, (d) three-ring focus, (e) anode.

Fig. 4.6

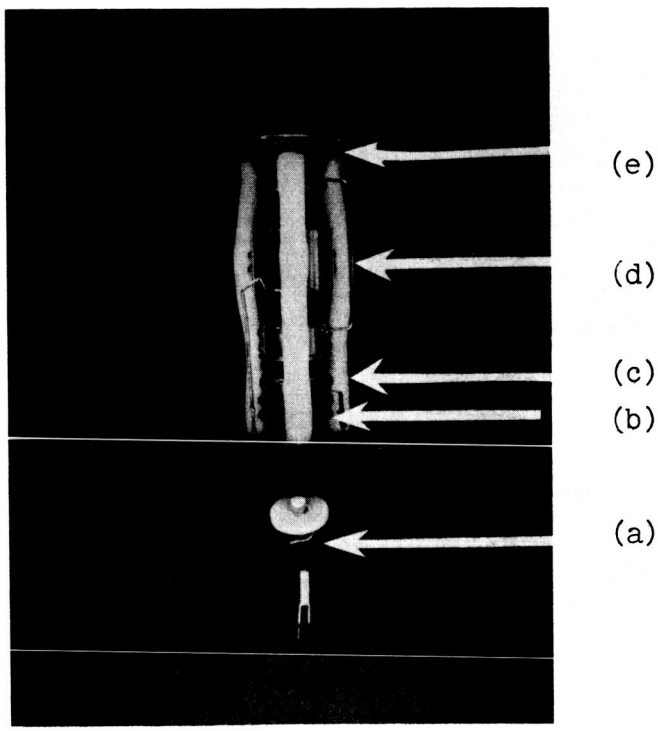
(e)
(d)
(c)
(b)
(a)

Because of the necessity of maintaining the scattering block at ground potential and referencing the energy of the electrons to the scattering block, the anode is at ground potential with the cathode being run at the desired negative potential. The electron gun is housed inside a metal vacuum container so as to be shielded from discharge magnetic fields and the gun housing is connected, at the anode end, to the scattering block through a metal bellows.

4.5 Spectroscopic Apparatus

The shock tube scattering block contains a set of apertures for the optical measurements located at right angles to the electron beam apertures. The bottom aperture is enclosed with a curved light trap constructed of a copper reducing elbow with a blackened inside surface. The top aperture is sealed for vacuum purposes with a quartz optical flat so that the plasma radiation can be visible through the scattering block. For convenience the emitted radiation is deflected at right angles by a front surface mirror and is then focused by a 24 in., f5.6 lens, on the entrance slit of the spectrograph. An f24 grating spectrograph* with a dispersion of 10.4 Ang/mm is used. The spectrograph was modified to perform time-resolved spectroscopy by substituting for the 35 mm film back, a photomultiplier box consisting of a beryllium-copper sheet with four slits milled in it. IP28 photomultipliers are located behind the slits to

* 1.5 Meter Bausch & Lomb Grating Spectrograph, Model No. 12 .

measure line and continuum intensities. The line slits are 16 Ang wide and are located to monitor the λ5876 of He I and the λ4686 line of He II. Two slits 33 Ang wide are located on either side of the λ5876 line to measure the continuum intensity. Because of space limitations, the continuum radiation is displaced with a parallel prism before entering the photomultiplier. The slit system is movable by means of an external screw and the position of the slit system is monitored by a dial guage. This allows an accurate means for setting the line position. A schematic drawing of the spectroscopic system is shown in Figure 4.7 .

Line broadening measurements were obtained by using a scanning monochromator of the Czerny-Turner type.** The instrument used is an f6.8, grating monochromator with a dispersion of 10 Å per mm. and a resolution of 0.2 Å . A 10 stage, end-on type photomultiplier is used to record the light intensity. Calibration of the instrument is accomplished by scanning the helium spectrum from a suitable Geissler tube.

** Spex Monochromator - 3/4 M focal length. Model No. 1700.

Schematic drawing of the spectroscopic system

Fig. 4.7

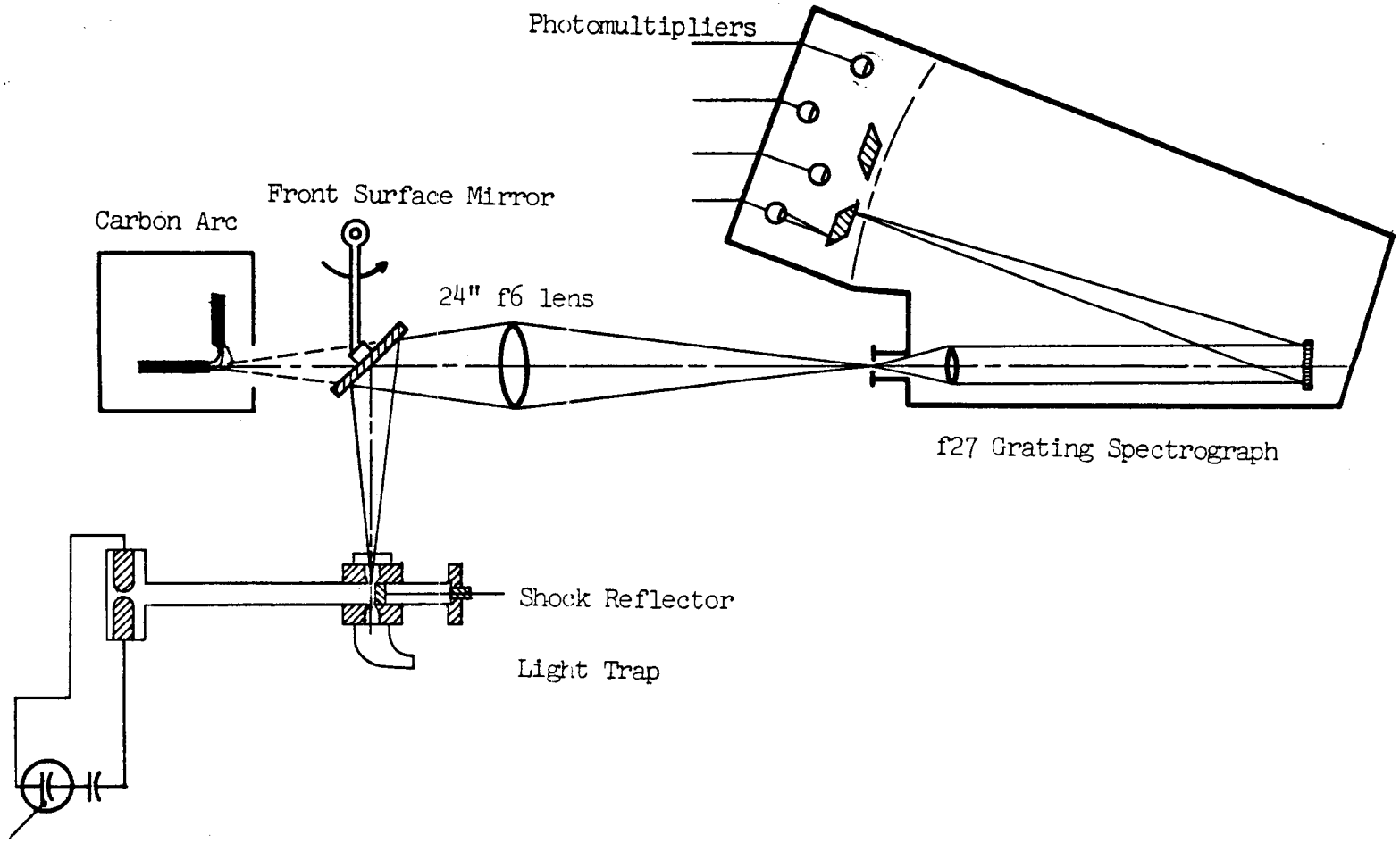
Photomultipliers
Front Surface Mirror
Carbon Arc
24" f6 lens
f27 Grating Spectrograph
Shock Reflector
Light Trap

4.6 Curved Electrostatic Energy Analyzer

A curved electrostatic analyzer*** was used for the energy loss measurements described in this experiment. It has the advantage of responding directly to the distribution of particle energies so that the output can be interpreted directly. The principal disadvantages are the small beam currents accepted by the entrance slit and the difficulty in construction.

The theory of operation of the curved electrostatic analyzer in elementary form [33] involves a force balance between the centrifugal force on a charged particle moving in a circular orbit and an oppositely directed radial electric force. In general, the electrostatic analyzer consists of two concentric cylindrical segments subtending an angle, ϕ .

For a given geometric ratio, r_2/r_1 , and an applied potential difference, V_o , between the cylindrical segments, a charged particle of the proper energy, E_o , can enter radially at the mean radius, r_o , and perform a circular orbit within the curved plates emerging at the same radius, r_o . An energy dispersion about E_o results in a radial dispersion of the emergence point about r_o . If a slit is placed at

---

*** A review of double focusing, mass spectrometers is presented in the work by Brunecke and Scherzer [34] .

the emergence point and the potential between the plates is varied, a distribution of energies, $E \pm \Delta E$, can be measured, where the spread, ΔE, is determined by the slit width. Such an instrument can be made to have a high resolution by using a small slit width and by ensuring that the particles enter tangentially at the mean radius r_o. A first-order focusing for particles entering with small radial displacements from r_o is obtained by making the angle $\phi = \frac{\pi}{\sqrt{2}}$.

The actual construction of a curved electrostatic analyzer is considerably more difficult than the theoretical considerations would imply. The curved plates do not exist isolated in space but must be maintained within a vacuum housing. The vacuum housing should be located as far away from the plates as possible to reduce the effects of the fringing fields. Another important consideration in the design of a practical analyzer is the elimination of axial effects by making the height of the curved plates much greater than the spacing between plates. The applied potential on the plates is generally balanced $\pm V_o/2$.

The most important consideration in analyzer construction is the location of the entrance and exit slits. The entrance slit system provides two functions. The first is to restrict the angular spread of the entrance beam and secondly to provide a termination to the fringe fields of the curved plates. The exit slit also must terminate the fringe field, and in the case of the $\frac{\pi}{\sqrt{2}}$ analyzer also determines the resolution. Most of the considerations mentioned

above were discovered after construction was completed and are mentioned in retrospect.

The analyzer entrance slit ($S_2 = \frac{1}{8}$") is located 3 cm. from the entrance to the deflection plates and is maintained at ground potential. The curved plates are constructed of spring beryllium-copper and are gold plated. Lucite forms, cut with two curved grooves at radii r_1, and r_2, hold the deflection plates in place at the top and bottom. The exit slit (S_3= .030 in) is located 1 in behind the exit plane of the curved plates and immediately behind the exit slit is placed the first dynode of an electron multiplier. The electron multiplier is constructed from a Du Mont type 6467, 10 stage multiplier phototube by removing the photocathode, and is used in a conventional manner with the first dynode at -1600 VDC and the anode signal appearing across a 1K load resistor to ground. The actual gain of the electron multiplier was not determined after removal of the photocathode, but it is estimated to be 10^4-10^5 . A detailed schematic of the energy analyzer and electron multiplier is shown in Figure 4.8 .

4.7 Data Recording and Experimental Procedure

Four channels of spectroscopic data are recorded simultaneously with the energy loss measurement so that the plasma conditions are known during the time of the measurement. A schematic drawing of the data system is shown in Figure 4.9 . An experimental data run is initiated with a trigger pulse to the ignitron after which the

Detail drawing of the curved, electrostatic
energy analyzer

Fig. 4.8

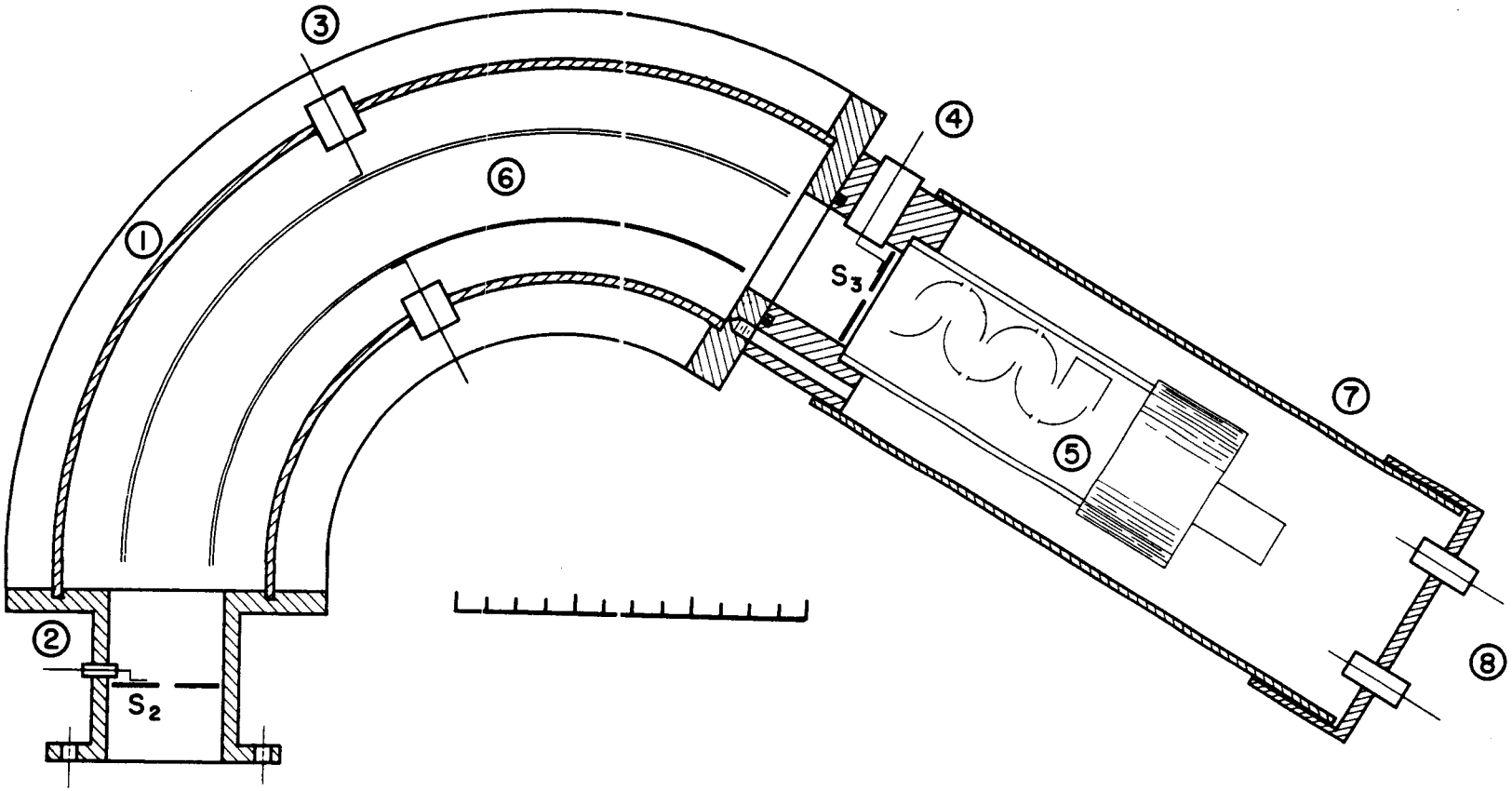
③
④
⑥
①
S_3
⑦
⑤
②
S_2
⑧

Schematic drawing of the data
recording system

Fig. 4.9

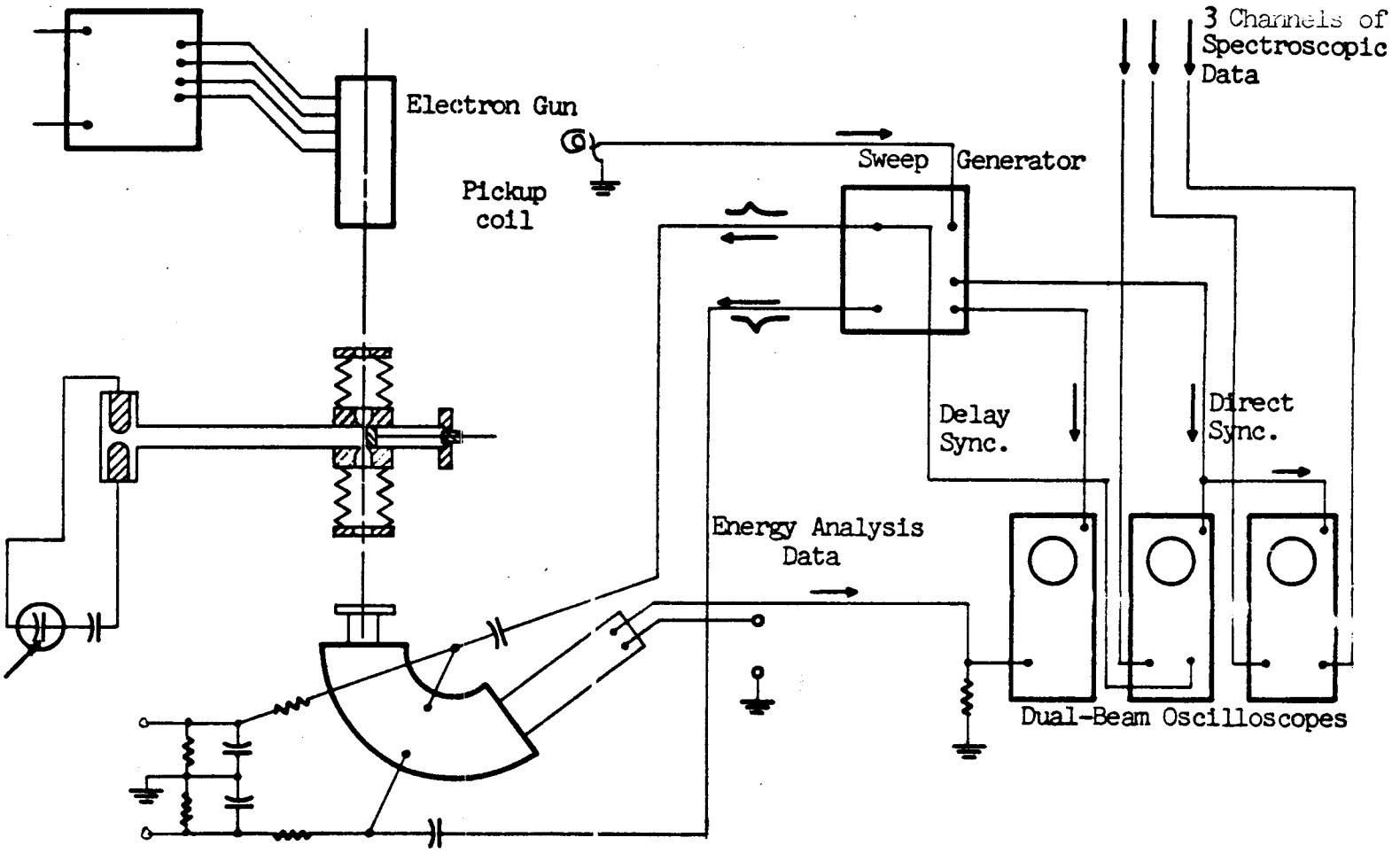
3 Channels of
Spectroscopic
Data
Electron Gun
Sweep Generator
Pickup
coil
Delay
Sync.
Direct
Sync.
Energy Analysis
Data
Dual-Beam Oscilloscopes

capacitor discharge of the "T" occurs. A magnetic pick-up coil senses the capacitor discharge and triggers the two oscilloscopes which record the spectroscopic data. At the same time a delayed ramp generator is triggered. After a predetermined delay which allows the shock wave to arrive at the scattering block the ramp generator turns on and produces a positive and negative set of linear voltage ramps of $\pm$120v for a duration of 3μ sec. which are applied to the energy analyzer. The ramp generator provides a delayed synchronizing pulse coincident with the start of the ramps which is used to trigger the oscilloscope that records the energy loss. One of the ramps is displayed along with the spectroscopic data. A typical set of data traces is shown in Figure 4.10 . In order to facilitate the energy loss measurement, a calibration response curve is recorded on the film previous to each data run. The relationship of the analyzer response to the voltage ramp is shown in Figure 4.11 . During a data run the shock tube is maintained at the operating pressure by a steady gas flow through the drift tubes with the electron beam running continuously.

A line profile measurement of the HeI, λ5016, line was performed by scanning across the line using repeated firings of the shock tube. Because of the long shock tube used in this experiment (100 cm.) and the low operating pressure (.35 torr) the shocks are not exactly reproducible from shot to shot. However, it was observed that shocks which have the same arrival time also exhibit the same absolute continuum intensity. The line was repeatedly

A typical set of data traces

(1) Continuum intensity at 5700 Ang
(2) HeI, λ5876 line radiation
(3) HeII, λ4686 line radiation
(4) Analyzer ramp monitor .35 torr, 11 KV, 10 μsec/cm time scale

Fig. 4.10

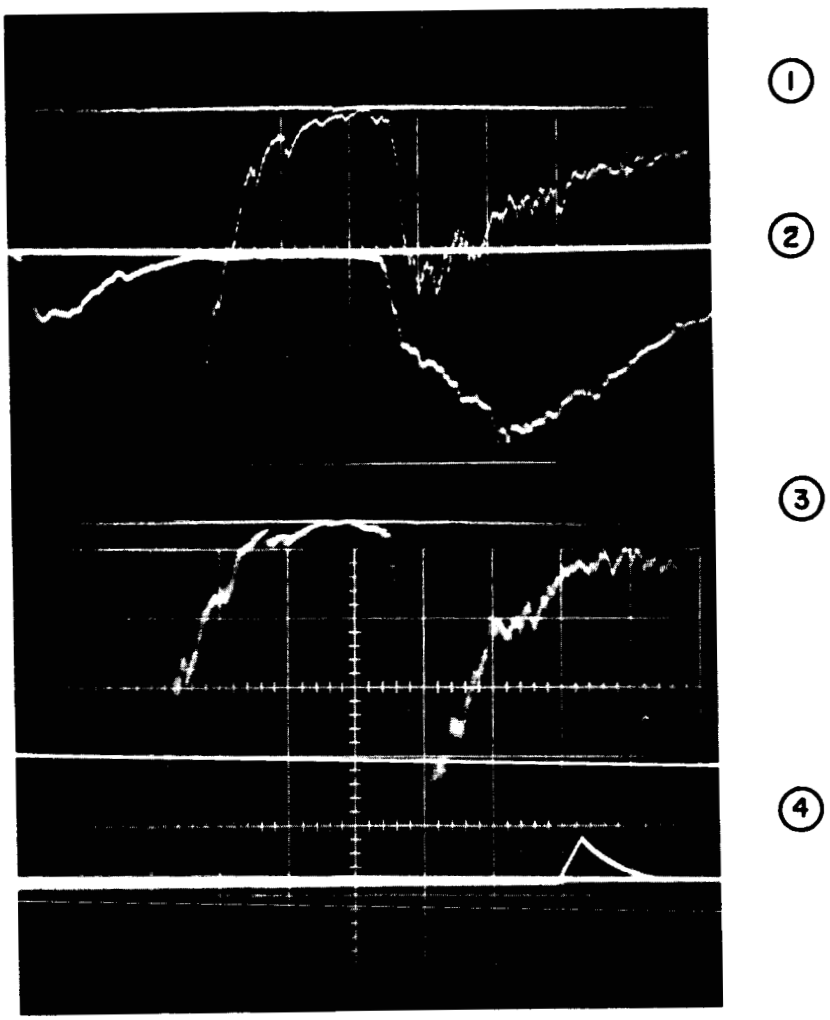
1
2
3
4

Oscillogram showing the linear voltage ramp and the associated analyzer response to a 3 kev electron beam. The time scale is .5μsec/cm.

Fig. 4.11

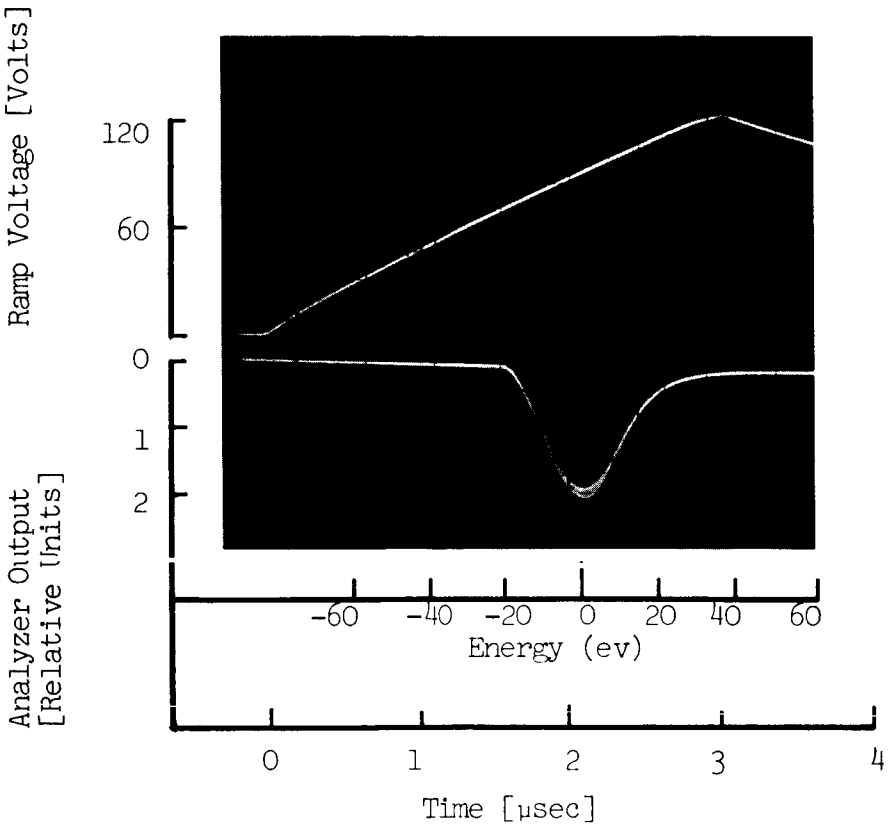
Ramp Voltage [Volts]
120
60
0
1
2
Analyzer Output
[Relative Units]
-60
-40
-20
0
20
40
60
Energy (ev)
0
1
2
3
4
Time [μsec]

scanned until sufficient data was obtained so that the traces could be grouped according to arrival time. The line profiles from shocks with the same arrival time are found to be reproducible. In this manner it is possible to obtain a line profile measurement to compare with known conditions of the energy loss measurements. A typical line profile measured during the experiment is shown in Figure 4.12 .

Measured HeI, λ5016 line profile

Fig. 4.12

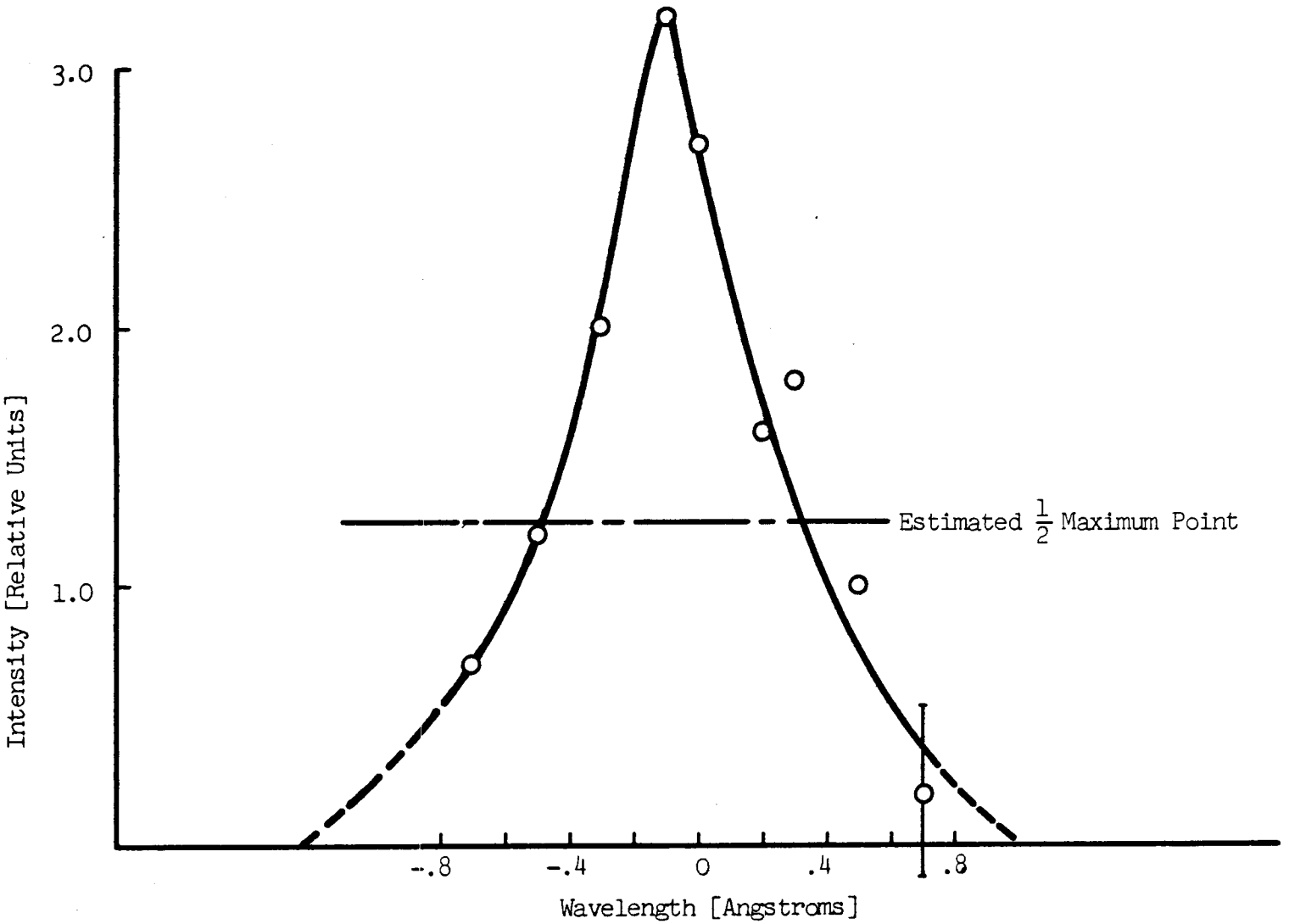
3.0
2.0
1.0
Intensity [Relative Units]
Estimated $\frac{1}{2}$ Maximum Point
-.8
-.4
0
.4
.8
Wavelength [Angstroms]

CHAPTER V

EXPERIMENTAL RESULTS AND ANALYSIS OF DATA

5.1 Spectroscopic Determination of Plasma Temperature and Electron Density

The plasma conditions are calculated from the photomultiplier traces at a time coincident with the ramp monitor signal (see Figure 4.10) . The measurements are performed in the reflected shock region so that plasma conditions are essentially constant during the energy analysis interval.

The plasma temperature is calculated by a relative intensity measurement which does not require an absolute intensity calibration. From the ratio of the HeI, $\lambda 5876$ line to the continuum intensity referenced to the same wave length, a temperature determination is made. The temperatures determined in this manner ranged from 35-40,000 ^{o}K for the data.

The plasma electron density is determined by an absolute continuum intensity measurement. For this measurement, an absolute calibration of the optical system is made using a carbon arc as an intensity standard.

Null and Lozier [35] show that, if the arc is operated in a specified manner, it is possible to maintain the crater luminance

equivalent to a variation in temperature of less than $\pm$ 10 ^{o}K . Under appropriate operating conditions the spectral radiance appears close to that typical of a blackbody of 3800 ^{o}K temperature throughout the spectral range 3000 to 42000 Angstroms. The spectral emissivity of the crater approaches unity over this spectral range with the true crater temperature close to 3800 ^{o}K .

In order to calibrate the entire optical system with the carbon arc, it is important to maintain identical optical geometries during the actual measurements as during the calibration. This is accomplished by locating the carbon arc in line with the spectrograph and lens system with the front surface mirror swung out of the way. A schematic of the optical system is shown in Figure 4.7 . Alignment of the optical system is accomplished by placing a light source at the exit focal plane of the spectrograph. The alignment light passes in opposite direction through the spectrograph and lens system and is deflected down through the optical flat so that finally the focussed dot is made to disappear into the light trap directly below at the lower side of the scattering block. This procedure ensures alignment of the spectrograph and also ensures that the light trap is directly behind the radiating volume of the plasma. The limiting aperture of the optical system is located at the entrance to the spectrograph. With alignment established, the mirror is swung out of the way and the carbon arc is positioned so that the test light is focussed at the center of the positive crater. A positive locking device is provided so that the mirror

returns to the same location each time.

The photomultipliers are calibrated *in situ* by using the carbon arc and a light chopper placed immediately in front of the spectrograph. Neutral density filters, calibrated at the same time, are used in the calibration. Linearity of the photomultipliers is checked by removing the neutral density filters and observing the variation of the output wave form of the chopped arc radiation.

The reflectivity of the front surface mirror was measured using a laser beam and a photodetector, and it is 80 per cent. The transmissivity of the quartz optical flat was measured to be 93 per cent.

The electron density was also determined during a separate experiment by a line profile measurement of the Stark broadened λ5016 line of HeI , as described in Section 4.4 . Because of the low light levels involved in this measurement, the entrance and exit slits of the grating monochromator were opened, with a resulting sacrifice in resolution. The instrumental line width was determined to be 0.6 Ang by measuring the full width at half maximum of the He, λ5016 line produced by an Osram lamp. The measured full width at half maximum of the Stark broadened line was corrected for instrumental broadening by assuming that the line shapes were Gaussian. The resolved line width of the broadened line was found to be 0.6 Ang. A plot of the line measurement is

shown in Figure 5.1 . The line broadening measurement was in reasonable agreement with the absolute continuum measurement and served the purpose of verifying the electron density measurements. The eleetron density varied from $5x10^{15}$ cm^{-3} to $1x10^{16}$ cm^{-3} during the data runs, as determined by the continuum measurements.

5.2 Energy Loss Measurements

The output of the energy analyzer indicates an energy loss ranging from 50 to 85 electron volts (ev) during the course of the experiment. The shift in the peak of the analyzer signal is used to determine the energy loss (this is a measurement of the most probable energy loss). A typical energy analysis trace is shown in Figure 5.2 where a one millimeter division on the trace corresponds to a loss of 7ev. In general the shift could not be measured more accurately than 7-10 ev so that the error in measurement is about 20% . The measurement of the width of the response curve contains considerably more error. The widths were corrected for the resolution of the analyzer by assuming that the line shapes are Gaussian. The resolved widths, which indicate the spreading in energy of the beam, range from 84 ev to 133 ev. The transmission of the beam during the data runs ranged from 0.3 per cent to 1.0 per cent of the incident beam current. A plot of the beam transmission as a function of electron density is shown in Figure 5.2a.

Measured line profile of HeI, λ5016 line

Fig. 5.1

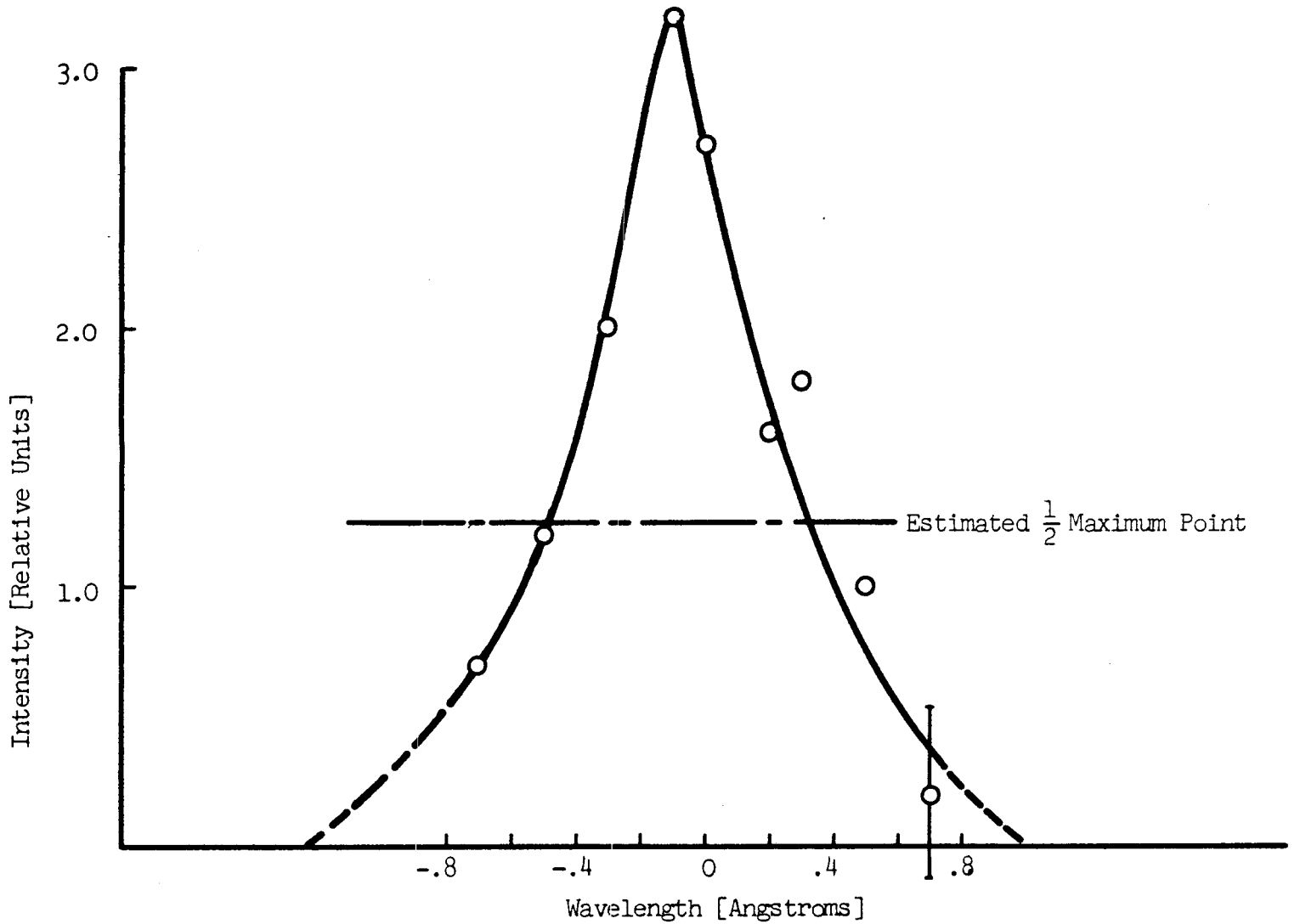
3.0
2.0
1.0
Intensity [Relative Units]
Estimated $\frac{1}{2}$ Maximum Point
-.8
-.4
0
.4
.8
Wavelength [Angstroms]

A typical energy analysis data trace

Fig. 5.2

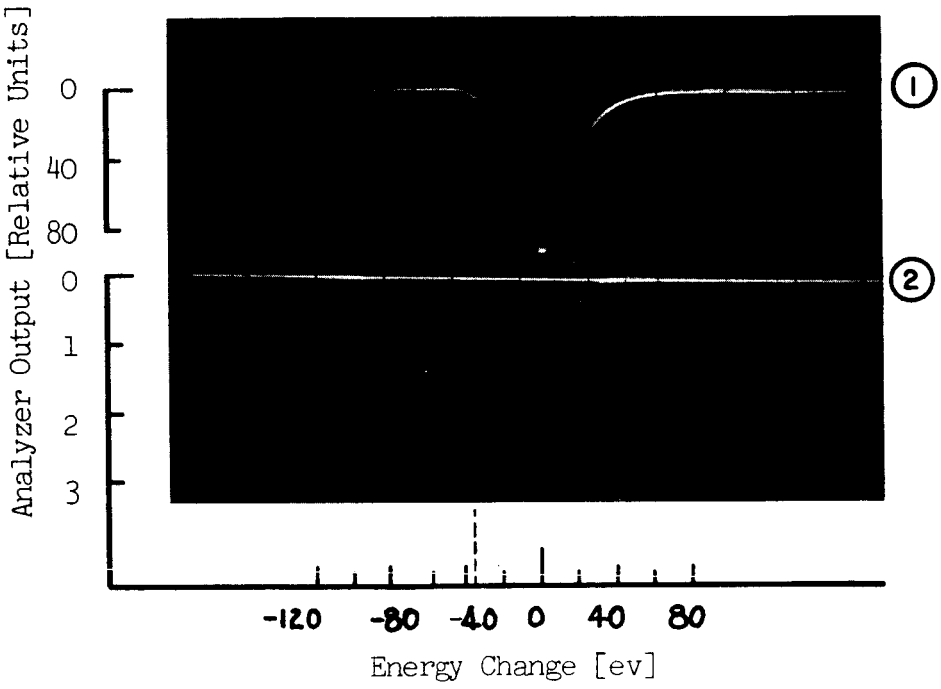

(1) Calibration, Response of Analyzer to 3 kev Beam
(2) Run, Response to 3 kev Beam through Plasma, $n_e = 6.4 \times 10^{15} cm^{-3}$

Measured beam transmission as a function of
plasma electron density

Fig. 5.2a

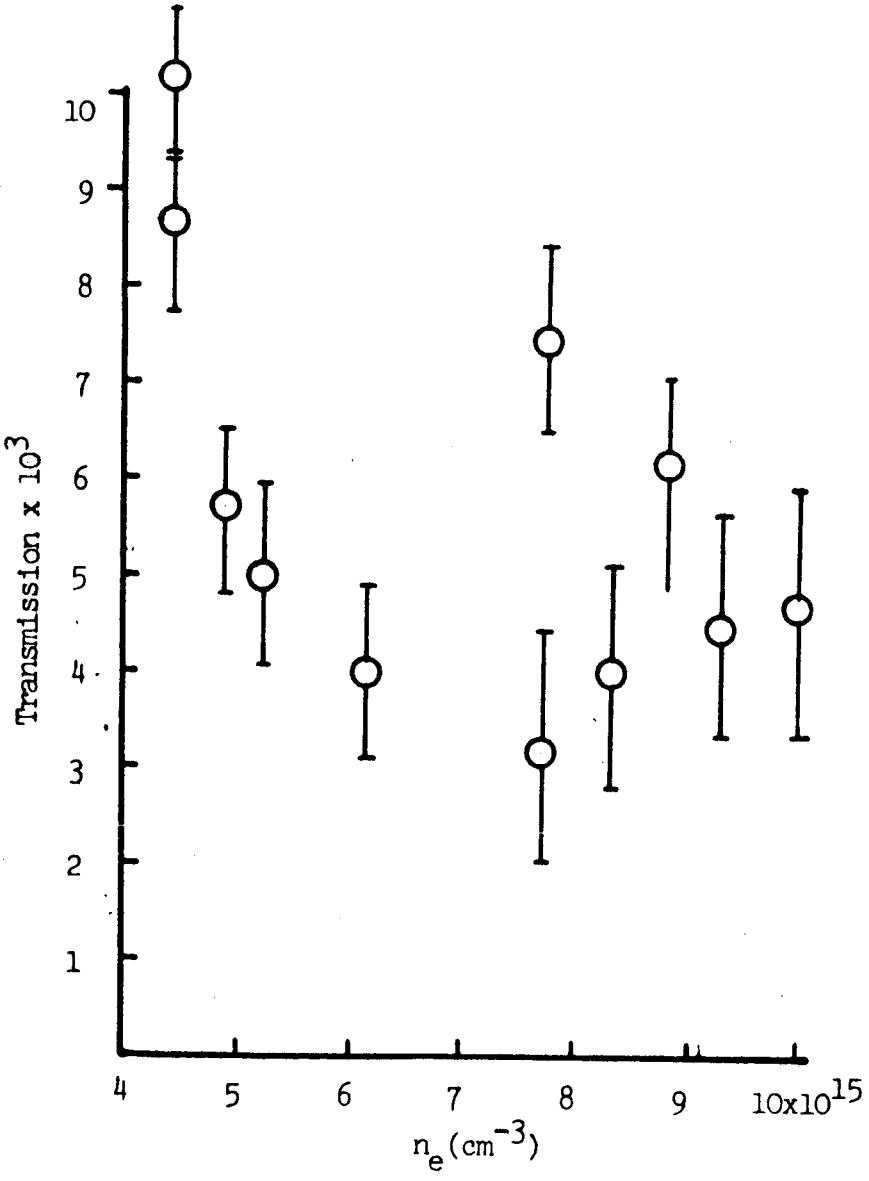
Transmission x 10^3
10
9
8
7
6
5
4
3
2
1
4
5
6
7
8
9
10x10^{15}
$n_e(cm^{-3})$

5.3 Comparison of Theoretical and Experimental Results

In Figure 5.3 the most probable energy loss, as determined by the shift of the analyzer peak, is plotted versus the plasma electron density. Within experimental error, the energy loss is proportional to the plasma electron density as the theory predicts. A comparison is made in Figure 5.4 of the experimental most-probable-energy losses with the theoretical most-probable-losses as derived from the Boltzmann equation solution. The experimental energy losses are approximately an order of magnitude higher than the theoretical predictions. The spread of energy losses as determined by the width of the resolved analyzer response is plotted versus plasma electron density in Figure 5.5 . It is seen that the energy spread also obeys a linear relationship with the density; however, the error in this measurement is large and it should be taken only to have qualitative significance.

In relation to the prediction of Kahn regarding electrons being accelerated and emerging with an energy greater than the incident energy, no such effect was observed.

5.4 Interpretation of the Experimental Results

The experimental energy losses are almost an order of magnitude higher than the theory predicts. There are three possible explanations which will account for the disagreement: A) the experimental measurements are in error, B) the theoretical model does not apply to the experimental conditions, C) the theory is

Experimental energy loss as a function of plasma electron density

Fig. 5.3

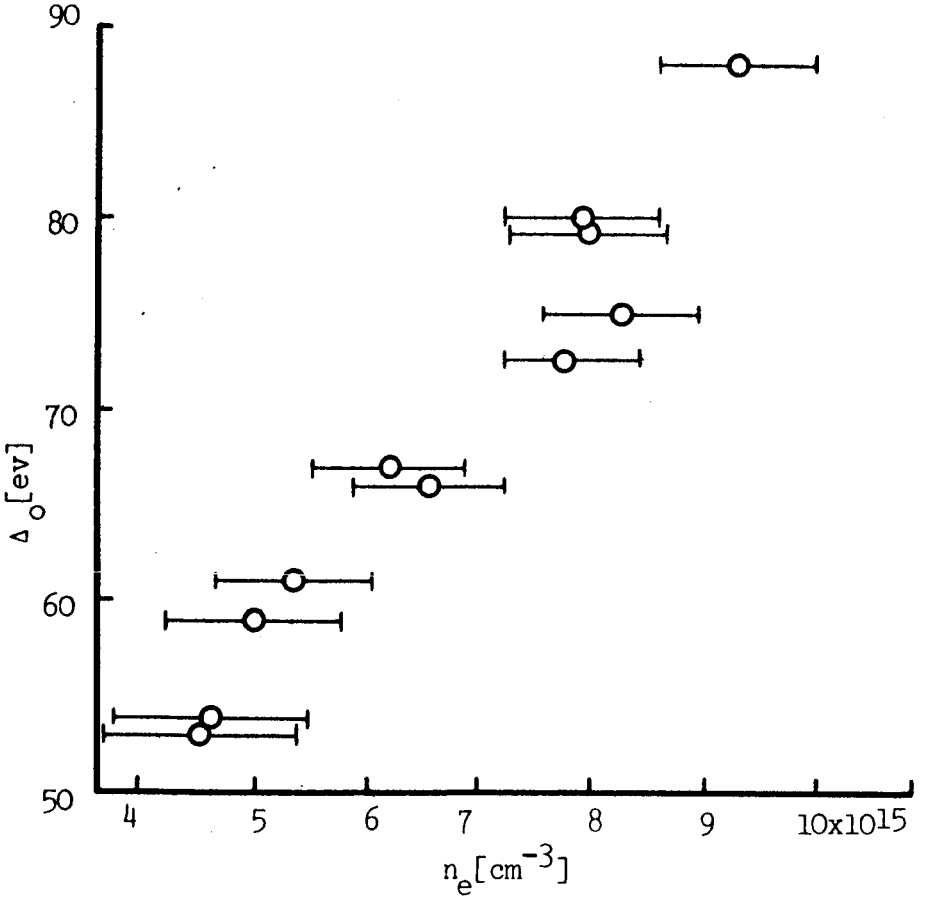
90
80
70
60
50
Δ_o[ev]
4
5
6
7
8
9
10x10^{15}
n_e[cm^{-3}]

Comparison of experimental and theoretical
energy losses

Fig. 5.4

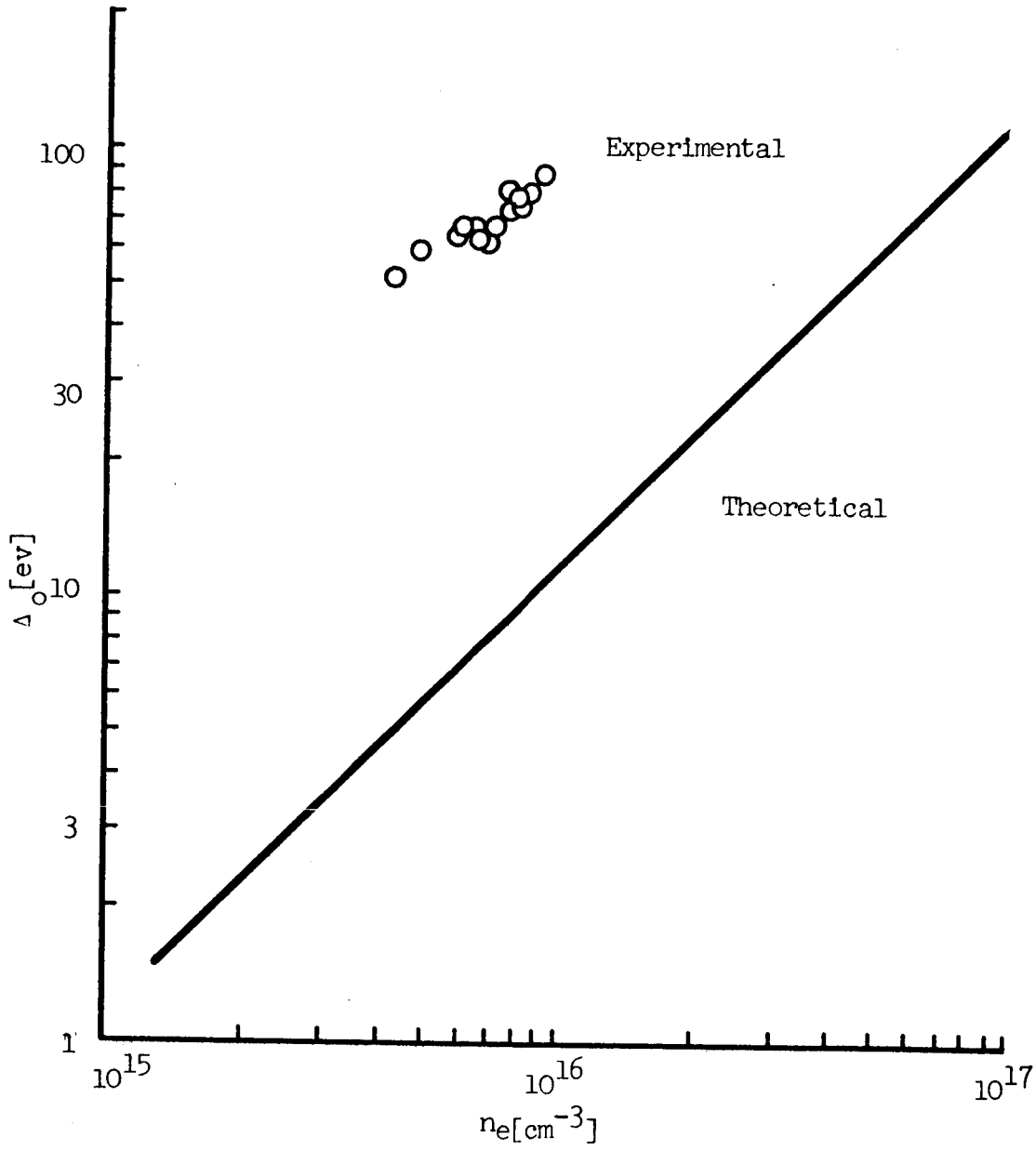
100
30
10
3
1
Δ_o[ev]
Experimental
Theoretical
10^{15}
10^{16}
10^{17}
$n_e[cm^{-3}]$

Experimental half width of the energy loss distribution as a function of plasma electron density

Fig. 5.5

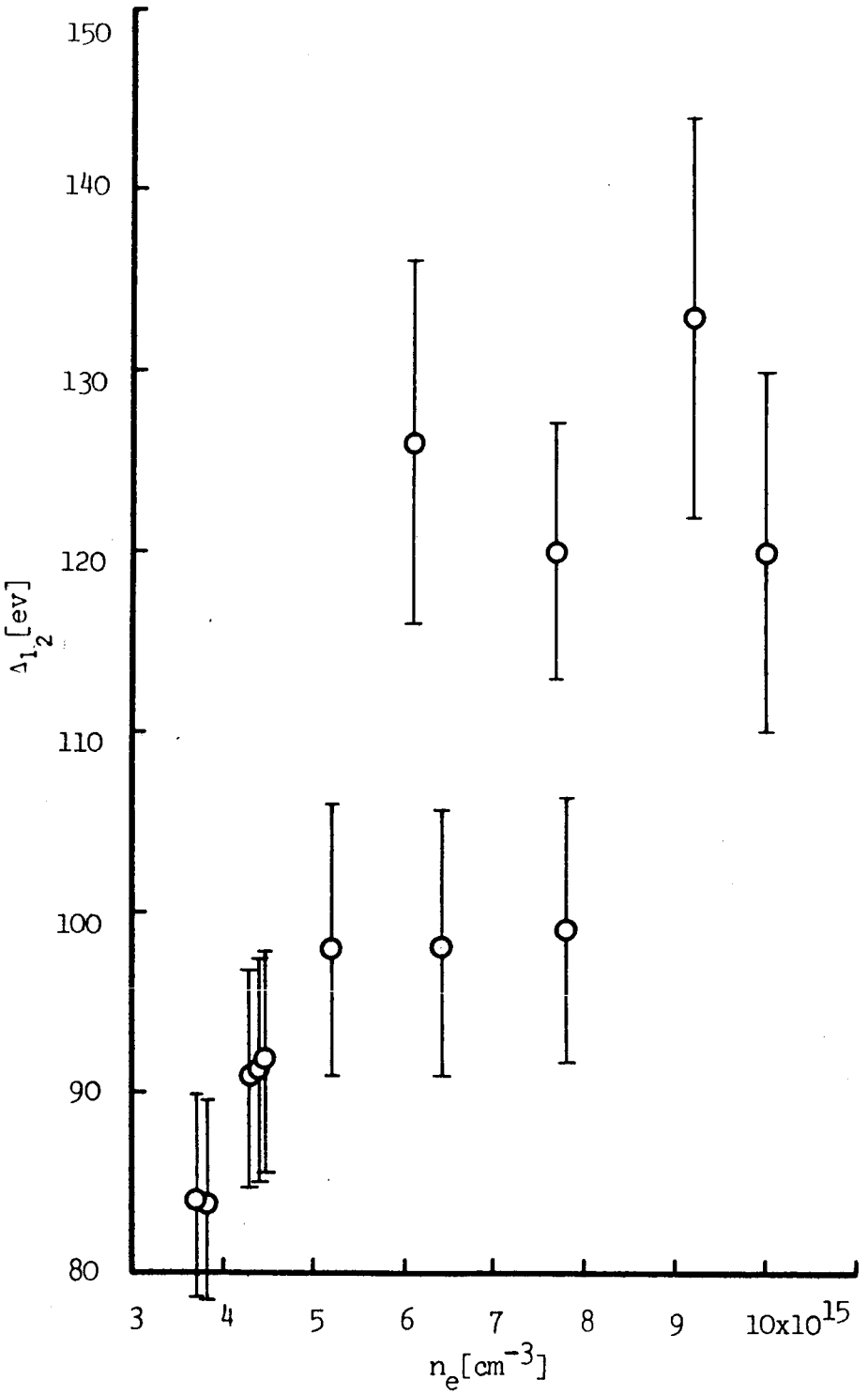
150
140
130
120
110
100
90
80
Δ_{1_2}[ev]
3
4
5
6
7
8
9
10x10^{15}
n_e[cm^{-3}]

inadequate. These possibilities are discussed in the following sections.

5.4-A Experimental Error

An error of almost an order of magnitude for the plasma electron density measurement is required for agreement with the theory. This is reflected as a required error of two orders (factor of 100) of magnitude in the absolute continuum measurement. The line profile broadening* of HeI, λ5016 is in good agreement with the absolute continuum measurements. The plasma electron density was calculated from an absolute continuum measurement, neglecting the effect of second ionization of the helium atoms. At the temperatures encountered in this experiment (~40,000°K) the fractional second ionization can be large enough to have an appreciable effect on the continuum measurement and calculation. (e.g., a 6% fractional second ionization increases the continuum intensity by 100%). The temperature was determined by a relative, atom-to-continuum measurement so that again, the second ionization effects cause an error in the temperature determination. These effects are circuitous so that the degree of fractional second ionization is difficult to estimate. It is important to note that the density determined by neglecting second ionization provides an upper limit to the actual

*The calculated full width at half maximum of HeI, λ5016 is ~0.6 Ang for $n_e=8\times10^{15}cm^{-3}$ and is approximately 5 Ang for $n_e=5\times10^{16}cm^{-3}$.

electron density. This upper limit is also substantiated by the line broadening measurements. The actual electron density could be significantly lower. In view of the discussion above, the actual discrepancy between the theoretical and experimental energy loss is somewhat uncertain. However, the discrepancy could be much worse than the results which are presented in Section 5.3 indicate.

In order to verify that the calibration of the analyzer was correct, an energy analysis was performed in the quiescent region immediately preceeding the arrival of the shock front. This procedure allowed a calibration to be made with no plasma present under identical conditions of the data run. The analyzer indicated a zero energy loss.

5.4-B Applicability of the Theoretical Model

The theoretical average energy loss is derived under the assumption of a single test electron interacting with a one-dimensional, infinite plasma. The experimental conditions must coincide with this model if the theory is to be applicable.

Typical electron beam currents are 100 μa at 3 kev energy and the corresponding beam density for a 2 mm diameter beam is $6 \times 10^{6} cm^{-3}$. The interaction volume for electron-electron collisions within the plasma is of the size of a sphere of radius $\lambda_D \frac{v}{w_t}$. For a plasma electron density of 10^{16} cm^{-3} and a temperature of 40,000 ^{o}K the interaction volume is 3×10^{-13} cm^{3}. The condition that only one

beam electron exists within the interaction volume is certainly satisfied, implying that there are no "bunching" effects in the beam.

The beam diameter is 2 mm and the plasma diameter is 2.5 cm so that the experimental conditions are one-dimensional.

The experimental conditions are accurately described as a plasma with vacuum boundaries since the existence of a sheath boundary is not feasible because of the extremely fast ambipolar diffusion rate at high temperatures. If a sheath is formed in front of the drift tubes with the arrival of the shock front, it will diffuse through the drift tube in .1μsec* resulting in a plasma vacuum interface at the time of the measurement. If sheaths did exist they should have a negligible net effect because of the symmetry of the shock tube. The sheath would decelerate the beam as it entered the plasma and cause an energy loss of the order of the plasma thermal energy. However, as the beam particles emerge from the plasma they will regain the energy through the exit sheath.

The possibility exists of having an electron density within the drift tubes, thus increasing the effective length of the plasma column. A calculation, based on the assumption that the plasma electrons would diffuse isotropically through the drift tubes at a

---

*This result is calculated using an ambipolar diffusion coefficient scaled to 40,000 ^{o}K. $D_a = 8 \times 10^3 cm^2/sec.$[36]

sound speed corresponding to the plasma temperature, indicated that the drift tube electron density would be two orders of magnitude lower than the plasma density within the shock tube.

Another possibility is that the effects are caused by a finite, bounded plasma. Experimental conditions have been chosen so as to approximate, as closely as possible, an infinite plasma. The length of plasma traversed by the electron beam is of the order of 10^6 Debye lengths. If the plasma column width were only a few Debye lengths, it is apparent that boundaries would be important. However, for the present experimental condition it is difficult to see quantitatively how the "finite" plasma could have an appreciable effect. The possibility of an effect due to the "finite" extent of the plasma is not ruled out completely, but it is difficult to understand how such an effect could produce the gross discrepancy between the theoretical and observed results.

5.4-C Inadequacy of the Theoretical Model

The evidence which has been presented indicates that the experimental determination of the plasma electron density, although subject to uncertainty, provides an upper limit to the electron density. The energy loss measurements are correct to within the stated experimental error. Arguments have been presented to show that there are no effects due to the drift tubes or to the plasma boundaries. The conclusion is that it would be desirable to review the theoretical considerations in search of additional energy loss

mechanisms.

There is certainly a strong justification for reconsidering with considerably more detail both the theory and the experiment.

CHAPTER VI

SUMMARY AND SUGGESTIONS FOR FUTURE WORK

6.1 Summary of Results

A collisional theory was developed for the average energy loss rate of an energetic test electron interacting with a plasma. Energy loss due to the excitation of plasma oscillations is accounted for in the theory through an *ad hoc* extension of the maximum impact parameter. The expression for the average energy loss rate obtained in this manner is in agreement with other available theories. An expression for the distribution of energy losses and for the transmission of the electron beam was also derived using a collisional theory.

An experimental determination was made of the distribution of energy losses of a beam of energetic test electrons traversing a plasma. The plasma conditions were determined independently using spectroscopic diagnostic techniques. The energy loss and the spread in energy losses were found to be proportional to the plasma electron density. The experimental energy loss was observed to be approximately an order of magnitude larger than that predicted by the available theory. In view of the uncertainty introduced in the electron density measurements, due to the effect of doubly ionized helium, the results obtained indicate a minimum discrepancy between theory and experiment. The actual discrepancy might be much worse.

The prediction of a high energy tail in the energy distribution, due to plasma acceleration mechanisms, was not substantiated by the experimental data.

6.2 Suggestion for Future Work

The present experimental work is limited to an extremely narrow range of the experimental parameters. Inadequate equipment forced this limitation. It would be desirable to extend the experiment over a larger range of the parameters, electron beam energy, electron beam density, plasma composition, plasma density and length of plasma. The difficulty in detecting small currents during short time intervals, placed the restriction on the upper range of plasma electron densities in the experiment. At densities above 10^{16} cm^{-3} the analyzer output was extremely small, and at densities of the order of 10^{15} cm^{-3} the energy loss becomes comparable to the analyzer error. The energy of the beam was restricted to a value $\geq$ 3,000 electron volts because at lower energies the beam transmission was reduced excessively. Energies much above 3 kev were not possible, simply because of inadequate high voltage connections. A more versatile electron gun would be needed in order to cover a substantial range of beam currents. The length of the plasma column traversed by the electron beams could be varied, within the same shock tube, by placing cylindrical inserts in the scattering block. In future experiments, an energy analyzer with a high energy resolution and with the capability of detecting smaller beam currents would allow the distribution of energy losses to be studied with

more precision.

The most serious limitation in the experiment was the difficulty in performing accurate spectroscopic diagnostics in helium at the temperatures and densities encountered ($n_e \approx 10^{16}$ cm^{-3}, T=40,000 ^{o}K) . In particular, the high temperature was responsible for low light levels from the atomic line radiation and for uncertainties in the continuum radiation due to the presence of doubly ionized helium. The diagnostics could be improved considerably by operating the shock tube at higher ambient pressures and by reducing the temperature. By the addition of 5-10 per cent hydrogen to the helium plasma, the temperature can be reduced to approximately 20,000 ^{o}K [37] . The temperature can be determined accurately in this range and a precise determination of the electron density could be made from simultaneous line profile measurements.

The effect of the capacitor discharge, magnetic field on the electron beam was eliminated by using a long shock tube and thereby performing the beam measurements after the oscillatory magnetic field had been fully damped. The shocks were not completely reproducible from shot to shot, due to the long tube and low ambient pressures. A shorter shock tube could be used (this would improve shot-to-shot reproducibility) if a distributed parameter, pulse forming network were used, rather than a single capacitor, to provide the discharge current. Such a pulsed discharge could be produced so that the discharge, magnetic fields would reduce to zero very rapidly.

The discrepancy which exists between the available theories and the experimental results obtained in this present work suggests that a theoretical program should be initiated in an attempt to explain the disagreement. Although the experiment was designed to satisfy the conditions of an infinite plasma it is still possible that the boundaries could influence the passage of energetic, charged particles.

After the refinements mentioned above have been thoroughly exhausted, and only then, the obvious extension of the experimental program would be to repeat the measurements in the presence of an applied magnetic field.

REFERENCES

1. S. T. Butler, M. J. Buckingham, Phys. Rev. 126 (1961)
2. N. F. Mott, Proc. Roy. Soc. (London) a126, 259 (1930)
3. R. I. Evans, The Atomic Nucleus, McGraw-Hill
4. L. Spitzer, Jr., Phys. of Fully Ionized Gases, Interscience
5. E. Everhart, et al, Phys. Rev. 99, 1287 (1955)
6. L. I. Schiff, Quantum Mechanics, McGraw-Hill (1955)
7. E. Fermi, Nuclear Physics (U. of Chicago Press, 1950)
8. J. Neufeld, R. Ritchie, Phys Rev 98, 1632 (1955)
9. Y. Klimentovich, J Sov Phys (JETP) 36, 999 (1959)
10. A. Akhiezer, Supp. al Nuovo Cimento III, Serie X (1956)
11. D. Pines, Phys Rev, 92, 626 (1953)
12. D. Pines, D. Bohm, Phys Rev, 85, 338 (1952)
13. A. Larkin, J Sov Phys (JETP), 37, 186 (1960)
14. D. Bohm, E. Gross, Phys Rev, 75, 1864 (1949)
15. G. Kalman, A. Ron, Ann Phys, 16, 118 (1961)
16. N. Rostoker, M. Rosenbluth, Phys Fluids, 3, 1 (1960)
17. E. R. Harrison, Phil. Mag 3, 1318 (1958); Plasma Physics (J. Nucl. Energy Part C) 1, 105 (1960); Plasma Physics (J. Nucl. Energy Part C) 4, 7 (1962)
18. H. Dricer, Phys. Rev. 117, 329 (1960)
19. J. D. Kahn, Astrophys. J., 129, 468 (1959)
20. W. A. Fowler et al, Astrophys. J Suppl. 2, 167 (1956)
21. Ya. B. Fainberg, Plasma Physics (Journal of Nuclear Energy, Part C) 4, 203 (1962)

REFERENCES

22. W. D. Getty, L. D. Smullin, J Appl. Phys, 34, 3421 (1963)

23. A. Akhiezer, Sov. Phys. (JETP) 13, 667 (1961)

24. M. R. Smith, Technical Report No. A-39 (Plasma Research, Case Institute of Technology, 1965)

25. R. S. Cohen et al, Phys Rev., 80, 230 (1950)

26. L. Landau, Journal of Physics, 8, 201 (1944)

27. H. F. Berg, et al, Phys Rev, 125, 199 (1962)

28. W. L. Weise, et al, Phys Rev, 129, 1225 (1963)

29. W. J. Karzas, R. Latter, Astrophys J., Suppl. 6, 167 (1961)

30. H. R. Griem, Phys. Rev. 128, 997 (o962)

31. H. R. Griem, Plasma Spectroscopy (McGraw-Hill, New York, 1964)

32. E. A. Mc Lean et al, Phys Fluids 3, 843 (1960)

33. W. W. Harman, Fundamentals of Electronic Motion, (McGraw-Hill, New York, 1953)

34. E. Brunecke, O. Scherzer, Geometrische Electron-Optic, (J. Springer, 1934)

35. M. R. Null, W. W. Lozier, J. Optical Soc. 52, 1156 (1962)

36. S. C. Brown, Basic Data of Plasma Physics, (Wiley, New York, 1959)

37. R. Lincke, Ph.D. Thesis, (University of Maryland, 1964)